

# Electronic decay process spectra including nuclear degrees of freedom

Alexander V. Riegel<sup>1,2</sup> and Elke Fasshauer<sup>1,2,3,\*</sup>

<sup>1</sup>*Center for Light-Matter Interaction, Sensors & Analytics (LISA<sup>+</sup>), University of Tübingen  
Auf der Morgenstelle 15, 72076 Tübingen, Germany*

<sup>2</sup>*Institute of Physical and Theoretical Chemistry, University of Tübingen  
Auf der Morgenstelle 18, 72076 Tübingen, Germany*

<sup>3</sup>*Department of Chemistry, University of Oxford, Oxford OX1 3QZ, United Kingdom*

(Dated: August 9, 2024)

In the field of chemistry, where nuclear motion has traditionally been a focal point, we now explore the ultra-rapid electronic motion spanning attoseconds to femtoseconds, demonstrating that it is equally integral and relevant to the discipline. The advent of ultrashort attosecond pulse technology has revolutionized our ability to directly observe electronic rearrangements in atoms and molecules, offering a time-resolved insight into these swift processes. Prominent examples include Auger-Meitner decay and Interparticle Coulombic Decay (ICD). However, the real challenge lies in interpreting these observations, where theoretical models are indispensable.

Building upon the analytical framework introduced in Phys. Rev. A 101, 043414 (2020), which analyzed the spectra of electrons emitted during electronic decay processes from a purely electronic perspective, our paper represents a significant advancement. We extend this theoretical base to include nuclear dynamics, utilizing the Born-Oppenheimer approximation to deepen our understanding of the intricate interaction between electronic and nuclear motion in these processes.

We illustrate the impact of incorporating nuclear degrees of freedom in several theoretical cases characterized by different numbers of vibrational bound states in both the electronic resonance and the electronic final state. This approach not only clarifies complex spectral features and unusual peak shapes but also demonstrates a method for extracting the energy differences between multiple vibrational resonance states through their distinctive interference patterns.

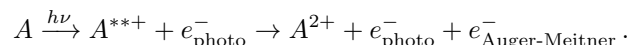
## I. INTRODUCTION

Since the advent of ultrashort laser pulses in the attosecond and femtosecond range [1], it has in principle become possible to study the time evolution of chemical reactions in detail. However, the duration of a laser pulse is inversely proportional to its energetic width and this width, for the current state of the art, needs to include at least one half-cycle of the mean photon energy. Hence, ultrashort laser pulses typically have mean photon energies in the extreme ultraviolet (XUV) or even x-ray range. We therefore aim to understand the processes initiated by these ultrashort laser pulses and what information we can extract from their respective time-resolved spectra.

The interaction of ultrashort laser pulses with matter prompts ionizations and excitations from the inner shells of atoms and molecules. The resulting excited states can then decay under electronic rearrangement and emission of an electron, which carries the excess energy. Such electronic decay processes have been known for many years. The Auger-Meitner process was discovered about 100 years ago [2, 3] and also the first theoretical prediction of the Interparticle Coulombic Decay (ICD) is more than two decades old [4].

The different electronic decay processes can be distinguished by the number of involved entities (atoms, molecules or weakly bound conglomerates) and the kind

of electronic rearrangement during the process. In the Auger-Meitner process, only one entity  $A$  is involved. After primary ionization from an inner shell, the vacancy is filled by an electron from an outer shell and another electron is emitted:



Here, we indicate an inner-shell vacancy by two stars  $**$ .

After an inner-shell excitation, the excited electron can either fill the vacancy itself and cause the emission of another electron (participator resonant Auger-Meitner process) or it can stay excited while another electron fills the vacancy and a third electron is emitted (spectator resonant Auger-Meitner process):



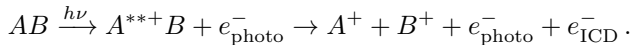
After the spectator Auger-Meitner process, the system is necessarily still excited and will decay further, whereas for the participator Auger-Meitner process with only one decay channel, this is not the case. However, when more channels are accessible, it is also possible to create an excited state, which will decay further.

The Auger-Meitner process is found in a variety of different systems like atoms, molecules and solids. As a consequence and because it is element specific, Auger-Meitner electron spectroscopy is used for surface analysis in metallurgy, quality analysis of microelectronics as

\* elke.fasshauer@gmail.com

well as for basic studies of chemical reaction mechanisms [5]. It has also been a test process for time-resolved measurements in general [6–8] and is often observed as a side product of modern x-ray spectroscopies [9].

In the ICD process, the energy released during the vacancy filling is transferred through space to a different entity, which consequently emits the ICD electron:



After the process, the two involved entities are both positively charged and therefore repel each other. The ICD process also has its resonant variants (resonant ICD, RICD), in analogy to the Auger-Meitner process.

ICD and ICD-like processes occur in many different systems with weakly interacting units such as noble gas clusters [10–13], proteins [14], solvents [11, 12, 15–20] as well as semi-conductors [21–23] and are discussed as a key mechanism of radiative DNA damage [24–28].

In this article, we will focus on the resonant electronic decay processes, which are initiated by inner-shell excitation rather than by ionization.

For time-resolved spectroscopy of electronic decay processes, most of the developed theory considers atomic systems [29, 30], for whose description the purely electronic Schrödinger equation suffices. However, for Auger-Meitner processes of molecules, molecules bound to a surface, like in heterogeneous catalysis, or an ICD process, the nuclear degrees of freedom will affect the spectra of the emitted electrons. Since numerical solutions of both the electronic and the nuclear dynamics are expensive to solve numerically, we aim for an analytical description following the basic formulation of Ref. [31], from which we can draw conclusions about basic properties. Moreover, by careful observation of the assumptions we make in our derivations, it will be possible to assign further properties observed in experiment to those parts which we neglect.

The analytical description of time-independent spectra of electronic decay processes dates back to the work by Fano [32]. His basic theory focuses on purely electronic wavefunctions. It has been generalized to quantum defect theory for molecules as well [33–37]. The latter has been investigated in a time-dependent approach for rotationally autoionizing states of the hydrogen molecule [38]. We will provide a similar ansatz for the wavefunction of a decaying state including both electronic and nuclear eigenstates of the system for non-interacting resonance states within the Born-Oppenheimer approximation, show general properties of the time-resolved spectra for selected cases and discuss the limits of our approach based on the approximations we introduce.

The article is structured as follows: In section II, we choose an ansatz for the Fano wavefunction including nuclear degrees of freedom for one electronic resonance and one electronic final state and derive the corresponding coefficients. We then derive the working expressions for the simulation and analysis of the time-resolved kinetic energy spectra of the emitted electron. In section III, we

have collected all the general parameters which we use to simulate the spectra for different showcases presented in section IV. We discuss the limitations and consequences of our introduced approximations in section V and summarize in section VI.

## II. THEORY

The electronic decay processes we intend to describe fully time-dependently are schematically illustrated in Figure 1 for the specific case of two nuclear bound states in the resonance state and one nuclear bound state in the electronic final state. The aim is to find a description for any combination of nuclear bound states in the electronic resonance and final states.

Starting from the ground state  $|G\rangle$ , we excite the system with an XUV pulse with a mean photon energy  $\Omega$  and thereby create a coherent superposition of the two nuclear states  $|\chi_\lambda\rangle$  of the electronic resonance state  $|r\rangle$ . The minimum of the potential energy curve is  $E_r$  and the energies of the nuclear states  $E_\lambda$  are determined relative to  $E_r$ . These resonance states can then, under emission of an electron, decay to a continuum state characterized by an electronic final state  $|E\rangle$  and a nuclear final state  $|\chi_\mu\rangle$  with a lifetime  $\tau_\lambda$ . The continuum states related to spectator resonant electronic decay processes can couple to other continuum states under emission of a photon. These processes are usually several orders of magnitude slower than the electronic decay process and are therefore neglected in this work. Alternatively to arriving in the continuum via a decaying resonance state, a simultaneous direct excitation and ionization (spectator) or a direct ionization (participator) channel is also possible, which is denoted "dir" in the figure.

From the derivations of Ref. [31], we know that the time-independent Fano wavefunction is essential to the description of the time-resolved spectra. We therefore first discuss the derivation of approximative Fano wavefunctions including nuclear degrees of freedom and afterwards derive the expression for the time- and energy-differential ionization probability.

### A. Derivation of the Fano coefficients including nuclear wavefunctions

Fano's purely electronic and time-independent wavefunction for one resonance and one final state is [32]

$$|\Psi_{\underline{E}}\rangle = a(\underline{E})|r\rangle + \int dE' b_{E'}(\underline{E})|E'\rangle. \quad (1)$$

Here,  $|r\rangle$  is the electronic wavefunction of the bound resonance state and  $|E'\rangle$  is the electronic continuum wavefunction including both the bound final state and the emitted free electron. Both are considered to be eigenstates of the Hamiltonian encompassing the operator of

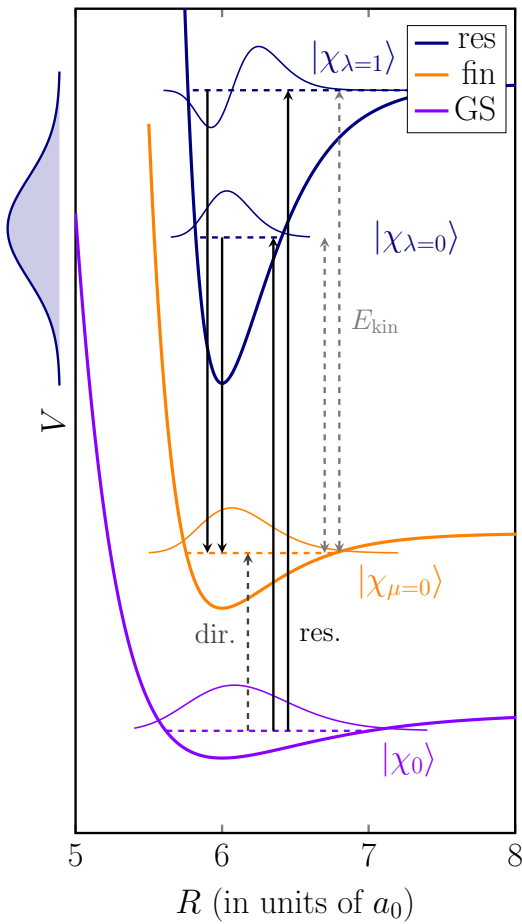


FIG. 1. (Colour online) Illustration [39] of the energy levels in the model systems used in this article. The three potential curves belong to the electronic ground state (lower curve in violet), final state (middle curve in orange) and resonance state (upper curve in dark blue). For each potential, the position of the bound vibrational eigenstates is indicated by dashed lines (here: one in both the electronic ground state and the final state, two in the resonance state, which corresponds to case 4 in section IV D) together with the corresponding vibrational eigenfunction and our chosen symbolic designation. The one-headed arrows depict possible pathways for the transition from the electronic ground state to the final state, either directly (dashed arrow) or via one of the vibrational eigenstates of the electronic resonance state (solid arrows). The double-headed arrow labelled " $E_{\text{kin}}$ " corresponds to the kinetic energy of the RICD electron emitted following the transition from the resonance state to the final state, in this case between the vibrational ground states. The Gaussian function on the left represents the initiating ultrashort laser pulse, which is energetically centred around the energy of the vibrational ground state of the electronic resonance state, relative to the electronic ground state.

the unperturbed system as well as the configuration interaction operator. The latter is mediating the electron-electron interaction which is causing the decay.  $a$  and  $b$  are coefficients, which are determined for the different cases.

We extend this ansatz to include nuclear degrees of freedom in the Born-Huang expansion [40] by adding a summation over the different nuclear eigenstates of the two respective potential energy curves. Hereby, we assume the electronic wavefunctions to be adiabatic wavefunctions.

$$|\Psi_{\underline{E}}\rangle = \sum_{\lambda} a_{\lambda}(\underline{E}) |r\rangle |\chi_{\lambda}\rangle + \sum_{\mu'} \int dE' b_{E',\mu'}(\underline{E}) |E'\rangle |\chi_{\mu'}\rangle \quad (2)$$

In order to determine the coefficients, we follow the same strategy as for the pure electronic Fano ansatz in Ref. [32] and solve the following set of equations assuming the Born-Oppenheimer approximation [41, 42].

$$\begin{aligned} \langle r | \hat{H} | \Psi_{\underline{E}} \rangle &= \sum_{\lambda} \langle r | \hat{H} a_{\lambda}(\underline{E}) | r \rangle |\chi_{\lambda}\rangle \\ &+ \sum_{\mu'} \int dE' \langle r | \hat{H} b_{E',\mu'}(\underline{E}) | E' \rangle |\chi_{\mu'}\rangle \\ &= \underline{E} \langle r | \Psi_{\underline{E}} \rangle \end{aligned} \quad (3)$$

$$\begin{aligned} \langle E'' | \hat{H} | \Psi_{\underline{E}} \rangle &= \sum_{\lambda} \langle E'' | \hat{H} a_{\lambda}(\underline{E}) | r \rangle |\chi_{\lambda}\rangle \\ &+ \sum_{\mu'} \int dE' \langle E'' | \hat{H} b_{E',\mu'}(\underline{E}) | E' \rangle |\chi_{\mu'}\rangle \\ &= \underline{E} \langle E'' | \Psi_{\underline{E}} \rangle \end{aligned} \quad (4)$$

Here, the Hamilton operator, as in Fano's ansatz, consists of the unperturbed Hamiltonian of the system,  $H_0$ , which involves both electronic and nuclear operators and is diagonal in the chosen electronic basis, and the purely electronic so-called configuration interaction operator  $V$  coupling the electronic resonance and continuum eigenstates with each other:

$$H_F = H_0 + V. \quad (5)$$

The vibronic eigenfunctions  $\{|r\rangle |\chi_{\lambda}\rangle\}$  and  $\{|E\rangle |\chi_{\mu}\rangle\}$  of  $H_0$  are characterized by their respective energies, which we choose to give as the sum of the minimum energy of the electronic potential energy curve plus the energy of the energy of the different vibrational levels ( $E_{r,\text{min}} + E_{\lambda}$  and  $E_{\text{fin},\text{min}} + E_{\mu}$ ). For a shorter notation, we will from here on denote them as  $E_r$  and  $E_{\text{fin}}$ . We assume that the coefficients are not explicitly dependent on either the electronic or the nuclear coordinates to obtain:

$$\begin{aligned} \langle r | \hat{H}_F | \Psi_{\underline{E}} \rangle &= \sum_{\lambda} a_{\lambda}(\underline{E}) (E_r + E_{\lambda}) |\chi_{\lambda}\rangle \\ &+ \sum_{\mu'} \int dE' b_{E',\mu'}(\underline{E}) V_{rE'} |\chi_{\mu'}\rangle. \end{aligned} \quad (6)$$

We project out the contribution of a single nuclear eigenfunction  $\langle \chi_{\lambda'} |$  and in doing so assume that the electronic configuration interaction term  $V_{rE'}$  does not directly depend on the nuclear coordinates. We have then

renamed  $\lambda' \rightarrow \lambda$  :

$$\begin{aligned} \langle \chi_\lambda | \langle r | \hat{H}_F | \Psi_{\underline{E}} \rangle &= a_\lambda(\underline{E})(E_r + E_\lambda) \\ &+ \sum_{\mu'} \int dE' b_{E',\mu'}(\underline{E}) V_{E'r} \langle \chi_\lambda | \chi_{\mu'} \rangle \\ &= \underline{E} a_\lambda(\underline{E}). \end{aligned} \quad (7)$$

Analogously, we obtain

$$\begin{aligned} \langle \chi_{\mu'} | \langle E' | \hat{H}_F | \Psi_{\underline{E}} \rangle &= \sum_{\lambda} a_\lambda(\underline{E}) V_{E'r} \langle \chi_{\mu'} | \chi_\lambda \rangle \\ &+ b_{E',\mu'}(\underline{E})(E' + E_{\mu'}) \\ &= \underline{E} b_{E',\mu'}(\underline{E}). \end{aligned} \quad (8)$$

---


$$(\underline{E} - E_r - E_\lambda) a_\lambda(\underline{E}) = \sum_{\mu', \lambda'} \mathcal{P} \int dE' \frac{a_{\lambda'}(\underline{E}) |V_{E'r}|^2 \langle \chi_\lambda | \chi_{\mu'} \rangle \langle \chi_{\mu'} | \chi_{\lambda'} \rangle}{\underline{E} - E' - E_{\mu'}} + \sum_{\mu', \lambda'} a_{\lambda'}(\underline{E}) |V_{(\underline{E}-E_{\mu'})r}|^2 z(\underline{E}) \langle \chi_\lambda | \chi_{\mu'} \rangle \langle \chi_{\mu'} | \chi_{\lambda'} \rangle. \quad (10)$$


---

An analytical closed form solution of this equation is not possible because only the decay of several resonance states to the same final state or the decay of one resonance state into several final states can be properly normalized in the way discussed by Fano [32]. In our case, the sum over  $\mu'$  or  $\lambda'$  prevents this normalization. We therefore make the assumption that the nuclear wavefunctions of the resonance state are not coupled via the continuum and hence introduce  $\delta_{\lambda,\lambda'}$ . This approximation is valid when the coupling of different nuclear resonance states is small or when, for a given  $\mu'$ , the Franck-Condon factor for  $\lambda$  is significantly larger than for all other values of  $\lambda'$ . Then, all contributions other than the one for  $\lambda' = \lambda$  are small and a large part of the sum is covered by the main contribution. We therefore limit the scope of this manuscript to so-called non-overlapping vibronic resonance states [43].

With this in mind, we deduce

$$z(\underline{E}) = \frac{\underline{E} - E_r - E_\lambda - \sum_{\mu'} F_{\mu'}(\underline{E})}{W_\lambda}. \quad (11)$$

Here,  $W_\lambda$  is the weighted sum of absolute squares of the configuration interaction terms of the different nuclear final states for a single nuclear resonance state

$$W_\lambda = \sum_{\mu'} |V_{(\underline{E}-E_{\mu'})r}|^2 |\langle \chi_\lambda | \chi_{\mu'} \rangle|^2 \quad (12)$$

$$\text{and } F_{\mu'}(\underline{E}) = \mathcal{P} \int dE' \frac{|V_{E'r}|^2 |\langle \chi_\lambda | \chi_{\mu'} \rangle|^2}{\underline{E} - E' - E_{\mu'}}.$$

Here, we have assumed that the electronic coupling matrix elements  $V_{(\underline{E}-E_{\mu'})r}$  are independent of the interparticle distance  $R$ . In reality, they exhibit a structure dependence, e.g., an exponential behaviour for Auger-Meitner processes or an  $R^{-3}$  dependence for ICD

By solving Eq. (8) for  $b_{E',\mu'}(\underline{E})$  we arrive at

$$\begin{aligned} b_{E',\mu'}(\underline{E}) &= \sum_{\lambda} \frac{a_\lambda(\underline{E}) V_{E'r} \langle \chi_{\mu'} | \chi_\lambda \rangle}{\underline{E} - E' - E_{\mu'}} \\ &+ \sum_{\lambda} a_\lambda(\underline{E}) V_{E'r} \langle \chi_{\mu'} | \chi_\lambda \rangle z(\underline{E}) \delta(\underline{E} - E' - E_{\mu'}). \end{aligned} \quad (9)$$

Here, we implicitly assume that the first part of the sum becomes the principal part upon integration over one of the energies. For only one resonance and one final state, we would insert this expression into Eq. (7) and solve for  $z(\underline{E})$ . However, when including nuclear wavefunctions, we arrive at

---

processes within the asymptotic approximation [44–47]. This effect will be discussed separately in a follow-up article.

Let us put this expression in Eq. (11) into perspective by comparing it to its purely electronic counterpart for the decay of one electronic resonance state to several electronic final states:

$$z_{\text{el}}(\underline{E}) = \frac{\underline{E} - E_r - \sum_f F_f(\underline{E})}{\sum_f |V_{rf}|^2}. \quad (13)$$

The similarities between them are obvious. The only difference is weighting the different decay widths by the Franck-Condon factors  $|\langle \chi_\lambda | \chi_{\mu'} \rangle|^2$ .

By again using  $\delta_{\lambda,\lambda'}$  consistently in the normalization of the wavefunction by calculating  $\langle \Psi_{\underline{E}} | \Psi_{\underline{E}} \rangle$  while, analogously to Fano, using

$$\begin{aligned} &\frac{1}{(\underline{E} - E' - E_{\mu'}) (E - E' - E_{\mu'})} \\ &= \frac{1}{\underline{E} - E} \left( \frac{1}{E - E' - E_{\mu'}} - \frac{1}{\underline{E} - E' - E_{\mu'}} \right) \\ &+ \pi^2 \delta(\underline{E} - E) \delta(E' - (E - E_{\mu'})) \end{aligned} \quad (14)$$

$$\begin{aligned} &\delta(\underline{E} - E' - E_{\mu'}) \delta(E - E' - E_{\mu'}) \\ &= \delta(\underline{E} - E) \delta(E' - \frac{1}{2}(\underline{E} + E - 2E_{\mu'})) \end{aligned} \quad (15)$$

and by assuming that  $F(\underline{E})$  is real, we obtain

$$\sum_{\lambda} |a_\lambda(\underline{E})|^2 W_\lambda (\pi^2 + |z(\underline{E})|^2) \delta(E - \underline{E}) = \delta(E - \underline{E}). \quad (16)$$

To solve this equation for the coefficient of only one vibrational eigenstate of the resonance state  $\lambda$ , we assume that the contributions of the different vibrational eigenstates are equally distributed amongst all  $N_\lambda$  vibrational bound states of the resonance state to give

$$|a_\lambda(\underline{E})|^2 W_\lambda (\pi^2 + |z(\underline{E})|^2) = 1/N_\lambda. \quad (17)$$

We finally determine the coefficients within the applied approximations to be

$$a_\lambda(\underline{E}) = - \frac{\sqrt{W_\lambda}}{\sqrt{N_\lambda} \sqrt{(\underline{E} - E_r - E_\lambda - \sum_{\mu''} F_{\mu''}(\underline{E}))^2 + \pi^2 W_\lambda^2}} \quad (18)$$

$$b_{E', \mu'}(\underline{E}) = \sum_{\lambda'} \frac{V_{E'r} a_{\lambda'}(\underline{E}) \langle \chi_{\mu'} | \chi_{\lambda'} \rangle}{\underline{E} - E' - E_{\mu'}} + \sum_{\lambda'} \frac{(\underline{E} - E_r - E_{\lambda'} - \sum_{\mu''} F_{\mu''}(\underline{E}))}{W_{\lambda'}} \frac{V_{E'r} a_{\lambda'}}{W_{\lambda'}} \delta(\underline{E} - E' - E_{\mu'}) \langle \chi_{\mu'} | \chi_{\lambda'} \rangle. \quad (19)$$

Because the  $F_{\mu'}(\underline{E})$  are small shifts in the energy position of the resonance state  $|r\rangle |\chi_\lambda\rangle$  caused by the interaction with the continuum, which are further damped by Franck-Condon factors, we neglect them in the following.

### B. Derivation of the time-dependent formulation for the description of time-resolved electronic decay spectra including nuclear degrees of freedom

The relevant property for the description of the time evolution of ICD processes is the time- and energy-differential ionization probability obtained from the time-dependent wavefunction  $|\Psi(t)\rangle$  by

$$P(E_{\text{kin}}, t) = \sum_i |\langle E_i | \Psi(t) \rangle|^2. \quad (20)$$

Here  $|E_i\rangle$  denotes a continuum state with energy  $E_i$ , which entails both the kinetic energy  $E_{\text{kin}}$  of the emitted electron and the energy of the final cationic state  $i$ . The electronic continuum states are orthogonal to all electronic bound states of the system and the nuclear eigenstates of each electronic state are orthogonal amongst each other. Atomic units are used throughout unless stated otherwise.

We obtain the wavefunction of the system by solving the time-dependent Schrödinger equation

$$i \frac{\partial}{\partial t} |\Psi(t)\rangle = H(t) |\Psi(t)\rangle \quad (21)$$

for the Hamiltonian

$$H(t) = H_0 + V + H_X(t). \quad (22)$$

Here,  $H_0$  is the Hamiltonian of the unperturbed system,  $V$  is the configuration interaction operator coupling resonance and continuum states and  $H_X$  describes the electro-magnetic field of the exciting laser pulse.

We are going to use the formalism of time-evolution operators  $U(t, t_0)$ , which adhere to a specific Hamiltonian and describe the propagation of a system from time  $t_0$  to time  $t$ :

$$|\Psi(t)\rangle = U(t, t_0) |\Psi(t_0)\rangle. \quad (23)$$

By using time-dependent perturbation theory, we can split off a small perturbation of the Hamiltonian from the rest

$$U(t, t_0) = \tilde{U}(t, t_0) - i \int_{t_0}^t dt' \tilde{U}(t, t') H^1(t') U(t', t_0), \quad (24)$$

where  $\tilde{U}(t, t_0)$  is the time-evolution operator of the system described by the zeroth order Hamiltonian  $\tilde{H}$  and  $H^1(t')$  is the first-order perturbation. As we will use this relationship twice and will redefine what is considered to be part of the unperturbed Hamiltonian operator, we start with this general expression.

Since the time-evolution operator  $U(t, t_0)$  appears on both sides of this integral equation, it can be solved iteratively by repeated insertion of Eq. (24) into itself:

$$U(t, t_0) = \tilde{U}(t, t_0) - i \int_{t_0}^t dt' \tilde{U}(t, t') H^1(t') \tilde{U}(t', t_0) + \mathcal{O}[(H^1)^2]. \quad (25)$$

The term up to first order is then given by:

$$|\Psi(t)\rangle = \tilde{U}(t, t_0) |\Psi(t_0)\rangle - i \int_{t_0}^t dt' \tilde{U}(t, t') H^1(t') \tilde{U}(t', t_0) |\Psi(t_0)\rangle. \quad (26)$$

We assume that the intensity of the exciting laser is so low that its interaction with the system can be described within the dipole approximation. Therefore, we can describe our system within first order of perturbation theory in  $H_X(t')$ . Starting from the ground state  $|G(t_0)\rangle$ , our wavefunction is given by

$$|\Psi(t)\rangle = \tilde{U}(t, t_0) |G(t_0)\rangle - i \int_{t_0}^t dt' \tilde{U}(t, t') H_X(t') \tilde{U}(t', t_0) |G(t_0)\rangle. \quad (27)$$

We are free to choose an energy reference and therefore select  $E_G = 0$ . This conveniently removes the time dependence from the ground state, since  $|G(t_0)\rangle = \exp\{-iE_G t_0\} |G\rangle = |G\rangle$ .

We introduce approximations for the time-evolution operator  $\tilde{U}(t, t')$  appearing in the last term of Eq. (27). After the system has interacted with the XUV via  $H_X(t')$  at time  $t'$ , the system decays via the configuration interaction  $V$ . In the continuum, we neglect the Coulomb interaction for simplicity, which leads to the time evolution operator

$$\tilde{U}(t, t') = U_0(t, t') - i \int_{t'}^t dt'' U_0(t, t'') V \tilde{U}(t'', t'), \quad (28)$$

where  $U_0(t, t')$  is the free-particle time-evolution operator.

By inserting Eq. (28) into Eq. (27) we arrive at

$$|\Psi(t)\rangle = \tilde{U}(t, t_0) |G\rangle - i \int_{t_0}^t dt' U_0(t, t') H_X(t') |G\rangle - \int_{t_0}^t dt' \int_{t'}^t dt'' U_0(t, t'') V \tilde{U}(t'', t') H_X(t') |G\rangle. \quad (29)$$

The time-evolution operator  $\tilde{U}(t'', t')$  in the last integral describes the contribution of the Hamiltonian  $H_0 + V$ . This is analogous to the Hamilton operator used in Fano's description [32] of a decaying resonance state and equivalent to the operator in Eq. (5). We therefore add the subscript F to the time-evolution operator and remove the tilde.

We now introduce the separation of electronic and nuclear wavefunctions. For the ground state, we assume the following product ansatz of the electronic wavefunction  $|g\rangle$  and the vibrational-ground-state wavefunction  $|\chi_0\rangle$ :

$$|G\rangle = |g\rangle |\chi_0\rangle. \quad (30)$$

In order to determine the probability amplitude for one specific final state, we project on one electronic continuum state  $|E\rangle$  and one vibrational state  $|\chi_\mu\rangle$  of this final state, characterized by their respective energies of the ionized system and the kinetic energy of the emitted electron. Inserting the resolution of the identity behind the time-evolution operator  $U_0$  in both the second and the third term on the right-hand side yields:

$$\begin{aligned} \langle \chi_\mu | \langle E | \Psi(t) \rangle &= \langle \chi_\mu | \langle E | U_F(t, t_0) | g \rangle | \chi_0 \rangle \\ &- i \int_{t_0}^t dt' \langle \chi_\mu | \langle E | U_0(t, t') H_X(t') | g \rangle | \chi_0 \rangle \\ &- \int_{t_0}^t dt' \int_{t'}^t dt'' \langle \chi_\mu | \langle E | U_0(t, t'') V U_F(t'', t') H_X(t') | g \rangle | \chi_0 \rangle \\ &= \langle \chi_\mu | \langle E | U_F(t, t_0) | g \rangle | \chi_0 \rangle \\ &- i \int_{t_0}^t dt' \sum_{\mu'} \int dE' \langle \chi_\mu | \langle E | U_0(t, t') | E' \rangle | \chi_{\mu'} \rangle \langle \chi_{\mu'} | \langle E' | H_X(t') | g \rangle | \chi_0 \rangle \\ &- \int_{t_0}^t dt' \int_{t'}^t dt'' \sum_{\mu'} \int dE' \langle \chi_\mu | \langle E | U_0(t, t'') | E' \rangle | \chi_{\mu'} \rangle \langle \chi_{\mu'} | \langle E' | V U_F(t'', t') H_X(t') | g \rangle | \chi_0 \rangle \end{aligned} \quad (31)$$

The time-evolution operator  $U_0(t, t')$  solves the time-

dependent Schrödinger equation for the Hamiltonian

$\vec{p}^2/2 + E_{\text{fin}} + E_\mu$ . The corresponding wavefunctions with wavevector  $\vec{k}$  are  $|\Psi_{\vec{k}}^0(t)\rangle = |\vec{k}\rangle \exp\left[-i \int_{-\infty}^t dt''' (\frac{1}{2}\vec{k}^2 + E_{\text{fin}} + E_\mu)\right]$ . Its projection formulation propagating a system from time  $t'$  to time  $t$  is given by

$$\begin{aligned} U_0(t, t') &= \int d\vec{k} |\Psi_{\vec{k}}^0(t)\rangle \langle \Psi_{\vec{k}}^0(t')| \\ &= \sum_{\tilde{\mu}} \int d\tilde{E} |\tilde{E}(t)\rangle |\chi_{\tilde{\mu}}(t)\rangle \langle \chi_{\tilde{\mu}}(t')| \langle \tilde{E}(t')| \\ &= \sum_{\tilde{\mu}} \int d\tilde{E} \exp\left[-i \int_{t'}^t dt''' (\tilde{E} + E_{\tilde{\mu}})\right] |\tilde{E}\rangle |\chi_{\tilde{\mu}}\rangle \langle \chi_{\tilde{\mu}}| \langle \tilde{E}|. \end{aligned} \quad (32)$$

At this point we only consider the kinetic energy of the emitted electron and can therefore write the projection of a general continuum state  $\langle E|$  on the free-particle time-evolution operator in the following way:

$$\begin{aligned} &\langle \chi_\mu | \langle E | U_0(t, t') | E' \rangle | \chi_{\mu'} \rangle \\ &= \int d\tilde{E} \sum_{\tilde{\mu}} \langle \chi_\mu | \langle E | \exp[i\Phi_0(E, t, t')] | \tilde{E} \rangle | \chi_{\tilde{\mu}} \rangle \\ &\quad \times \langle \chi_{\tilde{\mu}} | \langle \tilde{E} | E' \rangle | \chi_{\mu'} \rangle \\ &= \int d\tilde{E} \sum_{\tilde{\mu}} \langle \chi_\mu | \langle E | \tilde{E} \rangle | \chi_{\tilde{\mu}} \rangle \exp\left[-i \int_{t'}^t dt''' (\tilde{E} + E_{\tilde{\mu}})\right] \\ &\quad \times \langle \chi_{\tilde{\mu}} | \langle \tilde{E} | E' \rangle | \chi_{\mu'} \rangle \\ &= \exp\left[-i \int_{t'}^t dt''' (E_{\text{kin}} + E_{\text{fin}} + E_\mu)\right] \delta(E - E') \delta_{\mu, \mu'}, \end{aligned} \quad (33)$$

where  $E_{\text{kin}}$  is the kinetic energy relative to the final cationic state  $E_{\text{fin}} + E_\mu$  and  $\Phi_0(E, t, t')$  is the time-dependent phase.

The first term of the right-hand side of Eq. (31) vanishes because of the orthogonality between electronic bound and continuum eigenstates. The non-zero terms of Eq. (31) are given by

$$\begin{aligned} \langle \chi_\mu | \langle E | \Psi(t) \rangle &= -i \int_{t_0}^t dt' \exp\left[-i(t-t')(E_{\text{kin}} + E_{\text{fin}} + E_\mu)\right] \langle \chi_\mu | \langle E | H_X(t') | g \rangle | \chi_0 \rangle \\ &\quad - \int_{t_0}^t dt' \int_{t'}^t dt'' \exp\left[-i(t-t'')(E_{\text{kin}} + E_{\text{fin}} + E_\mu)\right] \langle \chi_\mu | \langle E | V U_F(t'', t') H_X(t') | g \rangle | \chi_0 \rangle. \end{aligned} \quad (35)$$

The second term can be solved by substituting the configuration interaction operator

$$\begin{aligned} \hat{V} &= \sum_{\mu'} \sum_{\lambda} \int dE' |E'\rangle |\chi_{\mu'}\rangle \langle \chi_{\mu'} | \chi_\lambda \rangle V_{E'r} \langle \chi_\lambda | \langle r | \\ &\quad + \sum_{\mu'} \sum_{\lambda} \int dE' |r\rangle |\chi_\lambda\rangle \langle \chi_\lambda | \chi_{\mu'} \rangle V_{rE'} \langle \chi_{\mu'} | \langle E' | \end{aligned} \quad (36)$$

and inserting the resolution of the identity

$$\begin{aligned} \mathbb{1} &= \sum_{\lambda'} |r\rangle |\chi_{\lambda'}\rangle \langle \chi_{\lambda'} | \langle r | \\ &\quad + \sum_{\mu''} \int dE'' |E''\rangle |\chi_{\mu''}\rangle \langle \chi_{\mu''} | \langle E'' | \end{aligned} \quad (37)$$

between the Fano propagator and the operator of the exciting field to yield

$$\begin{aligned}
& \langle \chi_\mu | \langle E | \Psi(t) \rangle = \\
& -i \int_{t_0}^t dt' \exp \left[ -i(t-t')(E_{\text{kin}} + E_{\text{fin}} + E_\mu) \right] \langle \chi_\mu | \langle E | H_X(t') | g \rangle | \chi_0 \rangle \\
& - \sum_{\lambda, \lambda'} \int_{t_0}^t dt' \int_{t'}^t dt'' \exp \left[ -i(t-t'')(E_{\text{kin}} + E_{\text{fin}} + E_\mu) \right] V_{Er} \langle \chi_\mu | \chi_\lambda \rangle \langle \chi_\lambda | \langle r | U_F(t'', t') | r \rangle | \chi_{\lambda'} \rangle \langle \chi_{\lambda'} | \langle r | H_X(t') | g \rangle | \chi_0 \rangle \\
& - \sum_{\lambda, \mu''} \int dE'' \int_{t_0}^t dt' \int_{t'}^t dt'' \exp \left[ -i(t-t'')(E_{\text{kin}} + E_{\text{fin}} + E_\mu) \right] V_{Er} \langle \chi_\mu | \chi_\lambda \rangle \langle \chi_\lambda | \langle r | U_F(t'', t') | E'' \rangle | \chi_{\mu''} \rangle \langle \chi_{\mu''} | \langle E'' | H_X(t') | g \rangle | \chi_0 \rangle .
\end{aligned} \tag{38}$$

Since we describe the interaction between the system and the exciting XUV field in the dipole approximation, the corresponding Hamilton operator in the length gauge is given by  $H_X(t') = -\mu \mathcal{E}_X(t') = \mu \frac{d}{dt'} A_X(t') f_X(t')$ , where  $\mathcal{E}_X(t')$  denotes the time-dependent field strength of the XUV laser, while  $\mu$  denotes the dipole operator,  $A_X(t') = A_{0X} \cos(\Omega t')$  is the vector potential of the laser

field in the direction of the linear polarization and  $f_X(t')$  is the Gaussian pulse envelope. We assume the transition dipole matrix element from the ground state to the continuum to be independent of the energy of the continuum state,

$$\langle E_i | \mu | g \rangle = \langle c | \mu | g \rangle, \tag{39}$$

over the energy range of interest:

$$\begin{aligned}
& \langle \chi_\mu | \langle E | \Psi(t) \rangle = \\
& + i \langle c | \mu | g \rangle \int_{t_0}^t dt' \exp \left[ -i(t-t')(E_{\text{kin}} + E_{\text{fin}} + E_\mu) \right] \langle \chi_\mu | \chi_0 \rangle \mathcal{E}_X(t') \\
& + \langle r | \mu | g \rangle \sum_{\lambda, \lambda'} \int_{t_0}^t dt' \int_{t'}^t dt'' \exp \left[ -i(t-t'')(E_{\text{kin}} + E_{\text{fin}} + E_\mu) \right] V_{Er} \langle \chi_\mu | \chi_\lambda \rangle \langle \chi_\lambda | \langle r | U_F(t'', t') | r \rangle | \chi_{\lambda'} \rangle \langle \chi_{\lambda'} | \chi_0 \rangle \mathcal{E}_X(t') \\
& + \langle c | \mu | g \rangle \sum_{\lambda, \mu''} \int dE'' \int_{t_0}^t dt' \int_{t'}^t dt'' \exp \left[ -i(t-t'')(E_{\text{kin}} + E_{\text{fin}} + E_\mu) \right] V_{Er} \langle \chi_\mu | \chi_\lambda \rangle \langle \chi_\lambda | \langle r | U_F(t'', t') | E'' \rangle | \chi_{\mu''} \rangle \langle \chi_{\mu''} | \chi_0 \rangle \mathcal{E}_X(t') .
\end{aligned} \tag{40}$$

The Fano matrix elements including nuclear dynamics require a thorough inspection. We assume a Born-Oppenheimer ansatz of the wavefunction, in which the electronic solutions are parametrically dependent on the

nuclear coordinates and the coefficients do not directly depend on either the electronic or nuclear coordinates. It is therefore possible to use the following projection formulation:



$$\begin{aligned}
U_F(t'', t') &= \int d\underline{E} |\Psi_{\underline{E}}(t'')\rangle \langle \Psi_{\underline{E}}(t')| \\
&= \int d\underline{E} |\Psi_{\underline{E}}\rangle \langle \Psi_{\underline{E}}| \exp[-i\underline{E}(t'' - t')] \\
&= \int d\underline{E} \exp[-i\underline{E}(t'' - t')] \left[ \sum_{\lambda'', \lambda'''} a_{\lambda''}(\underline{E}) a_{\lambda'''}^*(\underline{E}) |r\rangle |\chi_{\lambda''}\rangle \langle \chi_{\lambda'''}| \langle r| + \sum_{\lambda'', \tilde{\mu}} \int d\tilde{E} a_{\lambda''}(\underline{E}) b_{\tilde{E}, \tilde{\mu}}^*(\underline{E}) |r\rangle |\chi_{\lambda''}\rangle \langle \chi_{\tilde{\mu}}| \langle \tilde{E}| + \dots \right] \\
&= \int d\underline{E} \exp[-i\underline{E}(t'' - t')] \left[ \sum_{\lambda''} a_{\lambda''}(\underline{E}) a_{\lambda''}^*(\underline{E}) |r\rangle |\chi_{\lambda''}\rangle \langle \chi_{\lambda''}| \langle r| + \sum_{\lambda'', \tilde{\mu}} \int d\tilde{E} a_{\lambda''}(\underline{E}) b_{\tilde{E}, \tilde{\mu}}^*(\underline{E}) |r\rangle |\chi_{\lambda''}\rangle \langle \chi_{\tilde{\mu}}| \langle \tilde{E}| + \dots \right].
\end{aligned} \tag{41}$$

Because we assume that there is no coupling between nuclear eigenstates of the same electronic eigenstate via the continuum,  $\lambda''$  needs to be equal to  $\lambda'''$ .

As already mentioned, the derivation of the coefficients of Eqs. (18, 19) relies on several, in part crude, approximations. For a quantitative comparison to experiment, these should be checked carefully. However, they are fea-

sible for this qualitative description of the influence of nuclear dynamics on time-resolved spectroscopy on electronic decay processes. The Fano integrals can then be solved by contour integration in the negative complex half-plane as shown in Appendix A. Inserting them into Eq. (40) yields our working equation:

$$\begin{aligned}
\langle \chi_{\mu} | \langle E | \Psi(t) \rangle &= + i \langle c | \mu | g \rangle \int_{t_0}^t dt' \exp \left[ -i(t - t')(E_{\text{kin}} + E_{\text{fin}} + E_{\mu}) \right] \langle \chi_{\mu} | \chi_0 \rangle \mathcal{E}_X(t') \\
&+ \frac{\langle r | \mu | g \rangle}{N_{\lambda}} \sum_{\lambda} \int_{t_0}^t dt' \int_{t'}^t dt'' \exp \left[ -i(t - t'')(E_{\text{kin}} + E_{\text{fin}} + E_{\mu}) \right] \\
&\quad \times V_r \langle \chi_{\mu} | \chi_{\lambda} \rangle \langle \chi_{\lambda} | \chi_0 \rangle \exp \left[ -i(t'' - t')(E_r + E_{\lambda} - i\pi W_{\lambda}) \right] \mathcal{E}_X(t') \\
&- \frac{i\pi \langle c | \mu | g \rangle}{N_{\lambda}} \sum_{\lambda, \mu''} \int_{t_0}^t dt' \int_{t'}^t dt'' \exp \left[ -i(t - t'')(E_{\text{kin}} + E_{\text{fin}} + E_{\mu}) \right] \\
&\quad \times |V_r|^2 \langle \chi_{\mu} | \chi_{\lambda} \rangle \langle \chi_{\lambda} | \chi_{\mu''} \rangle \langle \chi_{\mu''} | \chi_0 \rangle \exp \left[ -i(t'' - t')(E_r + E_{\lambda} - i\pi W_{\lambda}) \right] \mathcal{E}_X(t').
\end{aligned} \tag{42}$$

The first part describes the direct ionization into the continuum final state, while the second part of Eq. (42) describes the excitation from the ground state to the resonance state followed by a decay to the continuum final state. The third part describes the excitation to a continuum state, which then couples to the resonance state, which then again decays into either the same or a different continuum final state.

The first integral thus corresponds to the direct ionization process. The second (double) integral is identical for the resonance and the indirect terms. They have, though, different prefactors and are weighted differently for the nuclear states. For the case of a slowly varying envelope function ( $\frac{d}{dt'} f_X(t') \approx 0$ ) and only considering the absorption of an XUV photon (neglecting the emission), these two integrals are solved analytically for times after the exciting pulse. The direct term for a specific value of  $\mu$  is given by

$$\begin{aligned}
& -\frac{A_{0X}\Omega\langle c|\mu|g\rangle}{2}\langle\chi_\mu|\chi_0\rangle\exp\left[-it(E_{\text{kin}}+E_{\text{fin}}+E_\mu)\right]\exp\left[-\frac{\sigma^2}{2}(E_{\text{kin}}+E_{\text{fin}}+E_\mu-\Omega)^2\right] \\
& \times\Re\left[\operatorname{erf}\left(\frac{1}{\sqrt{2}\sigma}\left(\frac{T_X}{2}+i\sigma^2(E_{\text{kin}}+E_{\text{fin}}+E_\mu-\Omega)\right)\right)\right],
\end{aligned} \tag{43}$$

where  $\Re$  denotes the real part and  $\operatorname{erf}$  denotes the error function. The resonance and indirect ionization terms

without their respective prefactors and weights are given by

$$\begin{aligned}
& -\frac{A_{0X}\Omega}{4(E_r+E_\lambda-i\pi W_\lambda-E_{\text{kin}}-E_{\text{fin}}-E_\mu)}\exp\left[-it(E_r+E_\lambda-i\pi W_\lambda)\right] \\
& \times\exp\left[-\frac{\sigma^2}{2}(E_r+E_\lambda-i\pi W_\lambda-\Omega)^2\right]\left(\operatorname{erf}(\tau_{1,\text{max}})-\operatorname{erf}(\tau_{1,\text{min}})\right) \\
& +\frac{A_{0X}\Omega}{4(E_r+E_\lambda-i\pi W_\lambda-E_{\text{kin}}-E_{\text{fin}}-E_\mu)}\exp\left[-it(E_{\text{kin}}+E_{\text{fin}}+E_\mu)\right] \\
& \times\exp\left[-\frac{\sigma^2}{2}(E_{\text{kin}}+E_{\text{fin}}+E_\mu-\Omega)^2\right]\left(\operatorname{erf}(\tau_{2,\text{max}})-\operatorname{erf}(\tau_{2,\text{min}})\right)
\end{aligned} \tag{44}$$

with  $\tau_{1,\text{max}} = \frac{1}{\sqrt{2}\sigma}\left(\frac{T_X}{2} - i\sigma^2(E_r + E_\lambda - i\pi W_\lambda - \Omega)\right)$ ,  
 $\tau_{1,\text{min}} = -\frac{1}{\sqrt{2}\sigma}\left(\frac{T_X}{2} + i\sigma^2(E_r + E_\lambda - i\pi W_\lambda - \Omega)\right)$ ,  
 $\tau_{2,\text{max}} = \frac{1}{\sqrt{2}\sigma}\left(\frac{T_X}{2} - i\sigma^2(E_{\text{kin}} + E_{\text{fin}} + E_\mu - \Omega)\right)$  and  
 $\tau_{2,\text{min}} = -\frac{1}{\sqrt{2}\sigma}\left(\frac{T_X}{2} + i\sigma^2(E_{\text{kin}} + E_{\text{fin}} + E_\mu - \Omega)\right)$ . Here,  $\sigma$  is the standard deviation of the Gauss distribution in time and  $T_X$  is the duration of the exciting XUV pulse. The different  $\tau$ 's are the upper and lower limits of the integral after the coordinate transformation that allows to formally solve the outer integral of the resonance and the indirect terms in Eq. (42).

The absolute square of the sum of all these terms gives the ionization probability for one specific nuclear final state. In order to determine the total spectrum, the contributions of all final states need to be added up according to Eq. (20).

### III. COMPUTATIONAL DETAILS

In the following, we will show the results for different cases with different numbers of nuclear bound states of either the resonance state or the final state, which were all obtained by the script `NUCLEAR_DYN` within a locally modified version of `ELDEST` [48, 49] (hash: 7dd1601).

We use Morse potentials in the simulations:

$$V_{\text{Morse}} = D(1 - \exp(-\alpha R))^2. \tag{45}$$

These are beneficial for our description because the vi-

brational wavefunctions are known analytically [50–52] and the evaluation of the Franck-Condon integrals is therefore possible without prior numerical solution of the nuclear Schrödinger equation. In our implementation, we use the recursive definition given in Eq. (49) of Ref. [53]. In order to compensate for the integration over  $R$  instead of  $\alpha R$  used in Ref. [53], we included an additional factor of  $\sqrt{\alpha}$  in the normalization constant.

However, the general findings, which we will discuss later, will also hold for other types of interatomic potentials.

Unless stated otherwise, the parameters of the Morse potentials were optimized for a given number of bound states, of which as many as possible have significant Franck-Condon overlaps between a) the ground and resonance state and b) the resonance and final state for equal equilibrium distances. Moreover, the energy differences between the vibrational ground state and first excited state are of the size usually found in existing chemical systems, especially diatomic molecules. We used  $\alpha_{\text{max}} = 30.0$  and  $D_{\text{max}} = 6.0$  eV and a purely electronic Fano  $q$  parameter of 1 [see Eq. (46)]. The electronic ground state is chosen such that it only contains one nuclear bound state and its parameters are kept constant. All parameters can be found in Table I.

We choose all configuration interaction terms  $V_r$  to be real and to correspond to a lifetime of  $\tau = \frac{1}{2\pi|V_r|^2} = 20$  fs to allow for an easier comparison between the different cases.

The electronic energies of the resonance states are chosen such that the energy difference between the vibrational ground state of the electronic ground state and the

TABLE I. Parameters of the Morse potentials defined in Eq. (45) and used for the simulations.

#	$\alpha_{\text{res}}$ [a.u.]	$D_{\text{res}}$ [eV]	$\alpha_{\text{fin}}$ [a.u.]	$D_{\text{fin}}$ [eV]
1	4.9512	0.01	21.6296	0.11
2	21.6296	0.11	17.0028	0.51
3	4.9512	0.01	4.9121	0.81
4	15.3994	0.50	21.7512	0.10
5	4.4414	0.04	23.9911	0.12
6	10.8894	0.50	5.1507	0.10
7	5.1507	0.10	10.8894	0.50

vibrational ground state of the resonance state has an energy of 50 eV. This allows us to use the same parameters for the initiating pulse, which is chosen to have a mean photon energy of 50 eV and  $n_X = 10$  cycles within the full width at half maximum (FWHM) of the Gaussian pulse. This results in an FWHM of 1.2 fs. The pulse is modelled for a total of  $5\sigma$ . Moreover, the electronic final state is chosen such that the secondary electron emitted during a transition from the vibrational ground states of the resonance state to the vibrational ground state of the final state is 10 eV.

In order to extract oscillation frequencies from the calculated time-resolved spectra, we employed a fast Fourier transform (FFT). To this end, we evaluated the signal for one specific kinetic energy, discarded the first eight data points to exclude the build-up phase from the signal and performed the FFT on the remaining data points. The central frequency of a peak was chosen as the centre of its FWHM.

#### IV. RESULTS

The basic findings for the purely electronic case have already been reported elsewhere [31]. We summarize them here, to allow a better comparison of the following showcases to the hitherto known case.

The shape of the signal after long times is a Fano profile convoluted with a Gaussian. The former's shape is described by the ratio between the contribution of the resonance part to the direct part of the wavefunction, which are included in the Fano parameter

$$q = \frac{\langle r | \mu | g \rangle}{\langle c | \mu | g \rangle \pi V_{Er}^*}, \quad (46)$$

so that the Fano profile may be described as

$$\frac{|\langle \Psi_E | \mu | g \rangle|^2}{|\langle E | \mu | g \rangle|^2} = \frac{(q + \epsilon)^2}{1 + \epsilon^2}, \quad (47)$$

where  $\epsilon = \frac{E_{\text{kin}} + E_{\text{fin}} - E_r}{\pi |V_{Er}|^2}$  (ignoring  $F(E)$ , as we do throughout this study) denotes a reduced energy variable [32].

The maxima and minima of the purely electronic Fano lineshape are given by

$$E_{\text{kin,max}} = E_r + E_\lambda - E_{\text{fin}} - E_\mu + \frac{\pi |V_{Er}|^2}{q} \quad (48)$$

$$E_{\text{kin,min}} = E_r + E_\lambda - E_{\text{fin}} - E_\mu - q\pi |V_{Er}|^2. \quad (49)$$

During the build-up of the Fano profile, oscillations in both energy and time are observed [31] originating from interference effects of the different pathways.

Moreover, the total lifetime of the resonance state can not be extracted from experimental data by a simple exponential fit, which assumes a sudden population of the resonance state. Instead, one needs to take the population of the resonance state over the entire pulse duration into account.

##### A. Case 1: 1 vibrational bound state in the electronic resonance state and 1 vibrational bound state in the electronic final state

This case, for which we used the parameters #1 of Table I for the simulation, is the most fundamental one. Since only one nuclear resonance state and one nuclear final state are considered, the derived and used expressions are exact within the limits of the Born-Oppenheimer approximation, the independence of the electronic bound-continuum coupling matrix element  $V_{Er}$  of the nuclear coordinates and the purely electronic Fano theory [31].

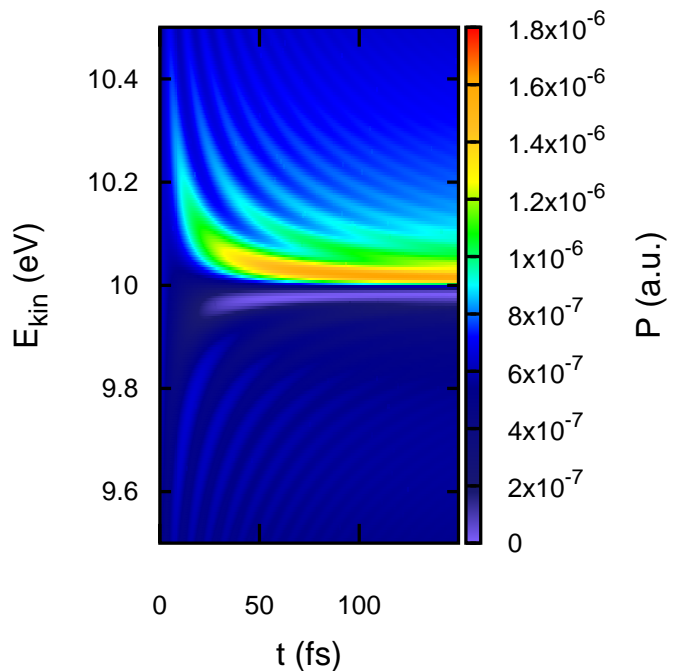


FIG. 2. (Colour online) Time-resolved kinetic energy spectrum of the RICD electron for one vibrational state in the electronic resonance state and one vibrational state in the electronic final state.

As to be expected from the purely electronic case, the spectrum contains a time-resolved build-up of a Fano profile convoluted by the Gaussian caused by the shape of the initiating laser pulse.

Including the nuclear degrees of freedom changes the details of the spectrum even in this most simple of cases. In our description, there are two main reasons for that.

Firstly, the effective decay width  $W_\lambda$  of this decay being 21.71 fs is slightly different from the purely electronic one of 20 fs. This deviation from the input lifetime is mainly artificial, though: According to Eq. (12), the decay width is weighted with  $|\langle \chi_{\lambda=0} | \chi_{\mu=0} \rangle|^2$ , the Franck-Condon factor between the vibrational resonance state and the vibrational final state. In this case, its value is 0.921. But analytical sum rules for Franck-Condon factors imply that for a given vibrational resonance state  $|\chi_\lambda\rangle$ , the sum of its Franck-Condon factors over all vibrational bound final states plus the integral of its Franck-Condon density over all vibrational continuum final states must equal unity. Given that only one bound final state exists in the example system examined in this case, the above figure of 0.921 already represents the bound-states term in the sum rule. On the other hand, vibrational continuum states are not considered in this study. This explains the missing 7.9% of Franck-Condon contributions. It should be noted, though, that even if vibrational continuum states of the final state were to be included, such states with an energy above the energy of the given vibrational resonance state would not contribute to the decay of the latter because the energy criterion for the RICD process would be violated for these channels. Thus in each instance, the lifetime of the resonance state will still be increased with respect to the purely electronic value, albeit to a much smaller extent than the one yielded by our present simulation.

Secondly, the shape of the signal is altered compared to the purely electronic one because the relative contributions of the different pathways are changed by the Franck-Condon overlaps.

Both effects, the Franck-Condon weighting leading to different relative contributions of the pathways and to an effective decay width  $W_\lambda$  (the latter being underestimated to some extent by neglecting continuum vibrational states), affect the lineshape of the kinetic energy distribution of the emitted electron. The shape still resembles a Fano profile, though, and we will discuss changes in peak shapes like the positions of minima and maxima based on an effective  $q$  parameter to make it comparable to literature in the field. It has to be noted, however, that this effective  $q$  parameter is not rigorously defined.

For a more narrow ground-state potential and shifted potential energy curves of the resonance and final states, the different classes of Franck-Condon overlaps (ground state - resonance state, ground state - final state and resonance state - final state) will in most cases be affected differently by alterations of the potentials in both width and shifts along the internuclear axis. As a result, the

direct, resonance and indirect pathways are weighted differently, which leads to a change in shape and amplitude of the peak. We won't discuss shifting of the potential energy surfaces along the internuclear axis in detail in the following, but we keep in mind that it can impact the individual peaks. In extreme cases, decay channels can become insignificant by shifting the potentials with respect to each other.

### B. Case 2: 1 vibrational bound state in the resonance state and 2 vibrational bound states in the final state

In this case, the parameters #2 of Table I were used for the simulation. Since only the final state has several vibrational bound states, the derived and used expressions are again exact within the limits of the Born-Oppenheimer approximation, the independence of the electronic bound-continuum coupling matrix element  $V_{Er}$  of the nuclear coordinates and the purely electronic Fano theory.

The total decay width is determined as the sum over the partial decay widths as given by Eq. (12). In this case, the effective decay width of 21.45 fs again deviates from the purely electronic one of 20 fs mainly due to incompleteness of the basis set of vibrational eigenfunctions. The sum of the Franck-Condon factors for the vibrational resonance state over both vibrational bound final states equals 0.941. The distance to unity is therefore smaller than in the previous case, which means that by ignoring the vibrational continuum states of the final state, a lesser error in the effective decay width is introduced in the present case.

The corresponding time-resolved spectrum shown in Figure 3 has two peaks with maxima at 10.015 eV and 9.785 eV corresponding to the transitions  $\mu = 0 \leftarrow \lambda = 0$  and  $\mu = 1 \leftarrow \lambda = 0$ , respectively.

We notice that the intensities of the two peaks differ and the overall spectrum is more complex than in case 1.

The corresponding Franck-Condon overlaps then determine the boost of the different decay peaks. In this particular case, they are  $\langle \chi_{\mu=0} | \chi_0 \rangle = 0.38$  and  $\langle \chi_{\mu=1} | \chi_0 \rangle = 0.82$ . Consequently, the direct contribution for the final state with  $|\chi_{\mu=1}\rangle$  is higher than that for the vibrational ground state.

The direct parts of the transition amplitudes also affect both the relative peak intensity and the peak shape of the corresponding decay peaks by changing the relative contributions of the direct, the resonance and the indirect terms. The other contributions are affected by the Franck-Condon overlaps involving the resonance state. In this example, they are  $\langle \chi_\lambda | \chi_0 \rangle = 0.87$ ,  $\langle \chi_{\mu=0} | \chi_\lambda \rangle = 0.55$  and  $\langle \chi_{\mu=1} | \chi_\lambda \rangle = 0.80$ . Since  $\langle \chi_{\mu=1} | \chi_\lambda \rangle$  is larger than  $\langle \chi_{\mu=0} | \chi_\lambda \rangle$ , the transition from the resonance state to the vibrational excited final state is favoured.

In order to determine the relative contributions of the different pathways to the respective signal, we need to

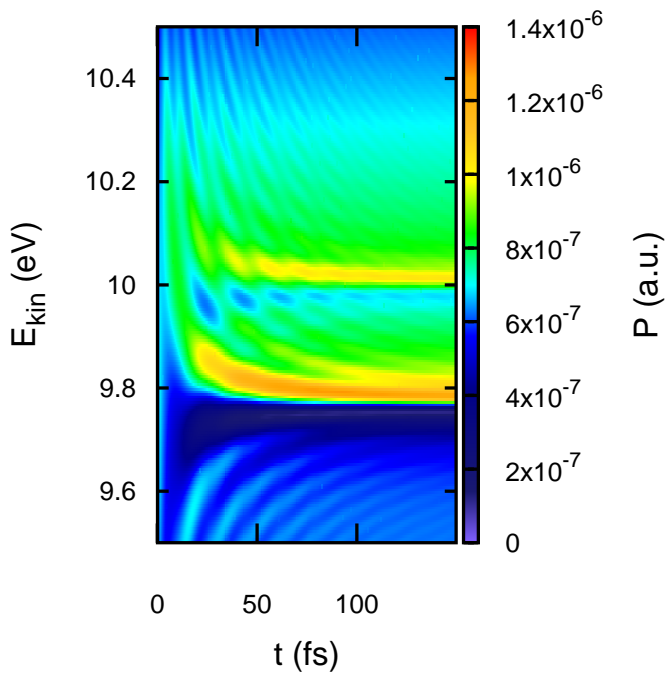


FIG. 3. (Colour online) Time-resolved RICD spectrum for one vibrational state in the electronic resonance state and two different vibrational states in the electronic final state. Two peaks are visible, one for each vibrational state in the final state. The peak at 10 eV corresponds to the vibrational  $0 \leftarrow 0$  transition, while the one at 9.8 eV corresponds to the  $1 \leftarrow 0$  transition. Both peaks exhibit the characteristic Fano profile. For a detailed discussion, see the main text.

compare  $\langle \chi_\mu | \chi_0 \rangle$  to the product  $\langle \chi_\mu | \chi_\lambda \rangle \langle \chi_\lambda | \chi_0 \rangle$  according to Eq. (42). These products are 0.48 ( $\mu = 0$ ) and 0.69 ( $\mu = 1$ ). Hence, for the vibrational ground state of the electronic final state with  $\mu = 0$ , the relative contribution of the resonance pathway is increased, while it is decreased for the vibrational excited state with  $\mu = 1$ . Qualitatively, this leads to the same effect as increasing an effective Fano parameter for the vibrational ground state of the final state and decreasing such an effective Fano parameter for the vibrational excited state. The minima and maxima of the peaks are shifted in energy with respect to a purely electronic  $q$  parameter. The maximum and minimum of the peak corresponding to the decay into the vibrational ground state of the electronic final state are shifted towards lower kinetic energies with respect to the energies expected for the purely electronic  $q$  parameter, while they are shifted towards higher energies for the peak corresponding to the decay to the vibrational excited state of the electronic final state.

During build-up of the signals, the interference-induced oscillations in time and energy of the two peaks overlap to yield a complex pattern. Despite the resulting additional oscillation pattern in time, this is not due to an additional interference effect, because the different final-state contributions are, according to Eq. (20), simply added up to yield the total spectrum.

A Fourier analysis of the oscillations in time for an exemplary kinetic energy of 9.6 eV shows two peaks with periods of 25 fs and 10 fs. They correspond to the interference between the resonance and the two direct pathways as already expected from the study of the purely electronic case [31].

### C. Case 3: 1 vibrational bound state in the resonance state and several vibrational bound states in the final state

In this case, the parameters #3 of Table I were used for the simulation of the time-resolved RICD spectrum shown in Figure 4. The final state has seven vibrational bound states with energies between 0.1158 eV and 0.8090 eV with respect to the electronic minimum energy. As for case 2, only the final state has several vibrational bound states, and therefore, the exactness is only limited by the same assumptions as in cases 1 and 2.

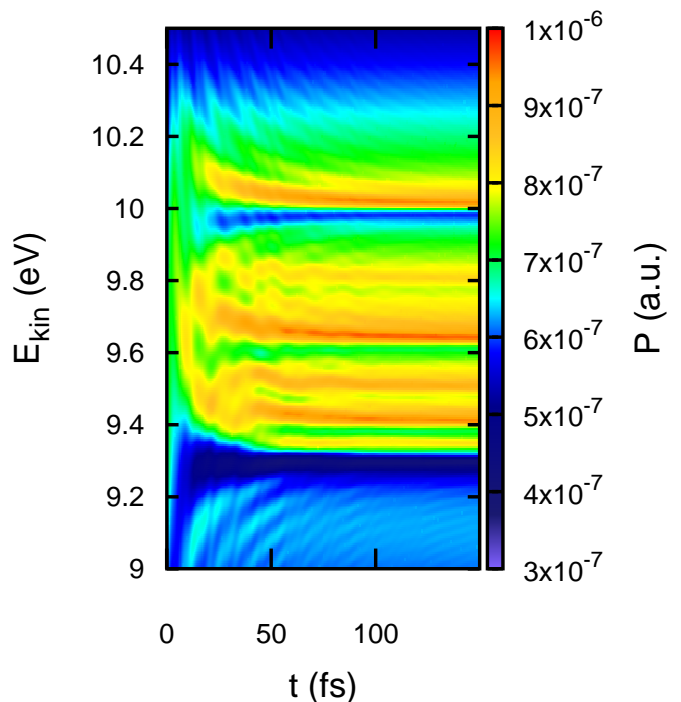


FIG. 4. (Colour online) Time-resolved RICD spectrum for one vibrational state in the electronic resonance state and seven vibrational states in the electronic final state.

Analogous to case 2, the overall spectrum is broadened towards lower kinetic energies by the possibility of ending in multiple vibrational final states. Moreover, the individual peak intensities and shapes are affected by the different Franck-Condon overlaps in the same way as in case 2. This is also reflected in the effective decay width of this case following Eq. (12), which corresponds to 20.28 fs, although the deviation with respect to the purely electronic case is, again, mainly due to the neglected contributions of vibrational continuum states. Consequently, the mani-

fold of signals yields a spectrum in which the oscillations in energy of the individual peaks become smeared out throughout the spectrum.

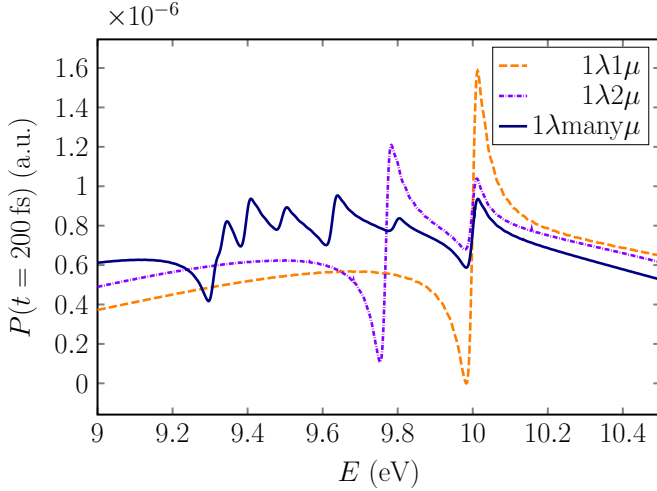


FIG. 5. (Colour online) RICD spectra at time  $t = 200$  fs for cases 1 (dashed curve in orange), 2 (dash-dotted curve in violet) and 3 (solid curve in dark blue).

Despite of having seven unique vibrational states in the electronic final state, only six clearly separated positive signals are visible. The two highest vibrational excited states are too close to be resolved and are instead combined into one peak as shown in the orange curve of Figure 5 at around 9.3 eV.

#### D. Case 4: 2 vibrational bound states in the resonance state and 1 vibrational bound state in the final state

This case provides the opportunity to discuss several features, amongst them the coherence between the two vibrational states in the resonance state. In order to give a thorough analysis, we have therefore chosen to display different sets of parameters.

##### 1. Large energy splitting between the vibrational resonance states, $q = 1$

In this case, the parameters #4 of Table I were used for the simulation. Here, the potential energy curve of the resonance state supports two vibrational bound states, which are split by 0.241 eV. The effective lifetimes of these two states are 111.93 fs and 37.67 fs for the vibrational ground and excited state, respectively. These are significantly larger than the input values for the purely electronic lifetime of 20 fs each. This may indicate a serious incompleteness of the vibrational eigenfunctions basis set, especially in the case of the vibrational ground state of the resonance state. However as of yet, we did

not quantify to which degree this prolongation of lifetimes is actually physical due to decay channels through high-lying states being energetically inaccessible.

The simulation with these parameters yields the spectrum shown in Figure 6. It is characterized by two peaks, corresponding to the vibrational states of the electronic resonance state. Contrary to cases 2 and 3, the signal corresponding to the vibrational excited state of the resonance state has a higher kinetic energy than the one corresponding to its vibrational ground state. Furthermore, the spectrum is not broadened by the possibility of exciting into several vibrational final states in the indirect pathway and, hence, the peak of the vibrational excited state of the electronic resonance state is slightly disfavoured by the energy profile of the laser pulse.

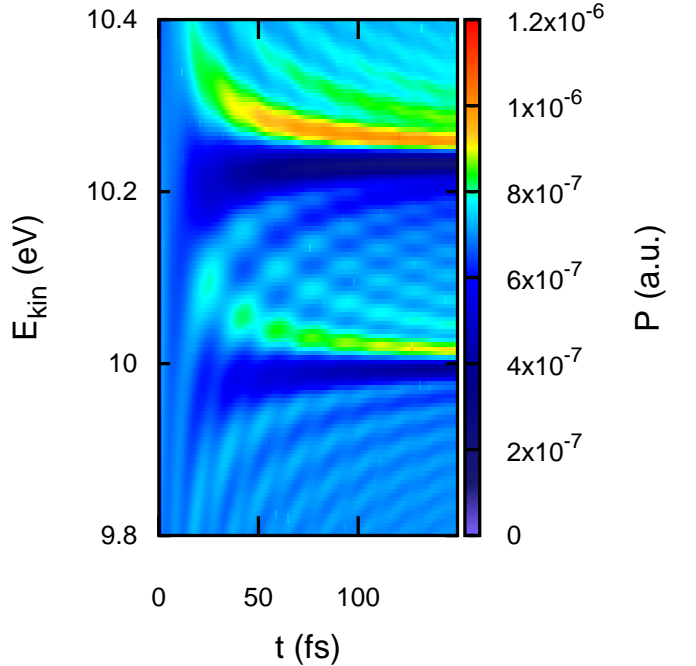


FIG. 6. (Colour online) Time-resolved RICD spectrum for two vibrational states in the electronic resonance state and a single vibrational state in the electronic final state. The peak at 10 eV corresponds to the vibrational  $0 \leftarrow 0$  transition, while the one at 10.2 eV corresponds to the  $0 \leftarrow 1$  transition. Both peaks again exhibit the characteristic Fano profile, plus an additional interference pattern created by the additional pathway via the vibrational excited state in the resonance state. For a detailed discussion, see the main text.

Again, the Franck-Condon parameters influence the peak intensity and shape, and since  $\langle \chi_\mu | \chi_0 \rangle = 0.91$  is significantly larger than both the products of  $\langle \chi_{\lambda=0} | \chi_0 \rangle = 0.38$  with  $\langle \chi_\mu | \chi_{\lambda=0} \rangle = 0.42$  and  $\langle \chi_{\lambda=1} | \chi_0 \rangle = 0.63$  with  $\langle \chi_\mu | \chi_{\lambda=1} \rangle = 0.73$ , the effective values of the Fano parameter are decreased. This favours the direct pathway relative to the pathway via the resonance state. Amongst the resonance pathways, the signal corresponding to the route via the vibrational excited state of the resonance state is significantly favoured over the one via its vibra-

tional ground state.

The overall spectrum has a complex pattern created by the interference of both the direct and resonance pathways. Moreover, in this case, it should also be possible to observe the interference between the pathways via the two different vibrational resonance states through an oscillation in time as per

$$P \propto \cos [(E_{\lambda=1} - E_{\lambda=0}) t] . \quad (50)$$

Figure 7 allows for a more detailed analysis of the interference pattern. It shows the oscillations in time at energies **a)** 10.12 eV, which is chosen to include the minima and maxima of the observed interference pattern of the spectrum, and **b)** 10.25 eV, which is close to the maximum of the peak corresponding to the pathway via the vibrational excited state of the electronic resonance state.

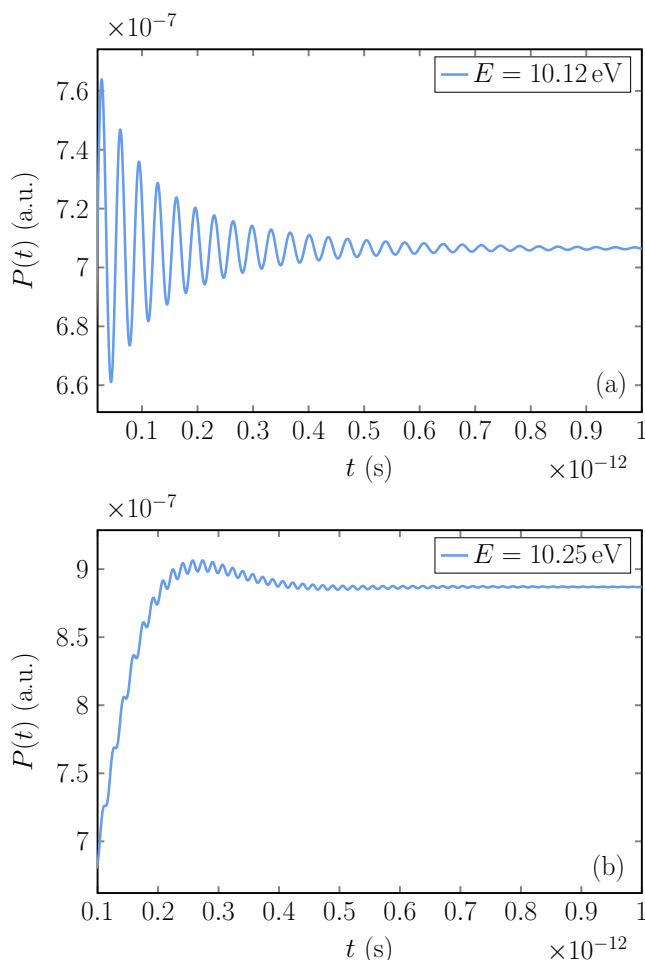


FIG. 7. Profiles in time for two vibrational states within the resonance state and one vibrational state within the final state (Figure 6). They have been evaluated at kinetic energies of **a)** 10.12 eV and **b)** 10.25 eV. A few data points which were affected by numerical noise have been discarded.

From earlier studies of time-resolved Fano profiles [29, 31, 54, 55], we know that for one resonance state, the

peak first builds up and then decreases exponentially according with the electronic decay. In Ref. [31], we showed that the interference between the direct pathway and the resonance pathway additionally leads to an oscillation in time, whose frequency is determined by the energy difference between the investigated energy of the cut through the spectrum and the theoretical resonance position.

For the case of two resonance states, irrespective of whether it is an electronic or a vibrational state, the interference between the contributions of the two resonance pathways to the wavefunction leads to another oscillation, whose period is determined by the energy difference between the two resonance states. Eq. (50) is an instance for such an oscillation. For the energy difference of this example, one would expect one cycle to last for 17 fs.

In Figure 7 **a)**, the cut between the peaks shows a clear oscillation in time with decreasing intensity. Its full period is 33.6 fs and hence twice the period one would expect for the resonance-resonance interference pattern. In Figure 7 **b)** with the cut close to the resonance, build-up occurs according to earlier studies. Overlaying this feature, an oscillation is visible which after ca. 200 fs has a stable period of 16.3 fs, close to the above theoretical value of 17 fs.

In neither case, the oscillation is caused by the resonance-resonance interference but rather by the interference of the direct with the respective resonance pathways. For the case of Figure 7 **a)**, considering the kinetic energy of 10.12 eV, the energy difference to the kinetic energy corresponding to the decay from the vibrational ground state of the resonance state is given by 0.12 eV corresponding to an oscillation period of 34.5 fs. This is in good agreement with the observed 33.6 fs. The relationship with the period of the resonance-resonance interference is only coincidental.

For the case of Figure 7 **b)** with a kinetic energy of 10.25 eV, the observed period almost equals the expected resonance-resonance interference period. However, at this kinetic energy, the period of the oscillation caused by the interference between the direct and the resonance parts of the neighbouring peak are the same as the period of the resonance-resonance interference. It is therefore not possible to distinguish between the two close to a resonance energy.

## 2. Large energy splitting between the vibrational resonance states, $q = 10$

In section IVD 1, the contributions of the resonance pathways were comparably small. Whether the resonance-resonance interference is strong enough to have an impact on the overall signal depends on both the intrinsic property of the  $q$  parameter — the larger  $q$ , the larger the resonance contribution — and the energetic width of the resonance part, which is inversely proportional to the temporal width and therefore also the number of cycles of the exciting pulse. It can hence be ma-

nipulated: the shorter the pulse, the larger the resonance signal at kinetic energies different from the peak maximum. This can directly be seen by inspection of the second part of Eq. (44). In order to highlight the resonance-resonance interference and its properties, we increase the purely electronic Fano parameter  $q$  from 1 to 10.

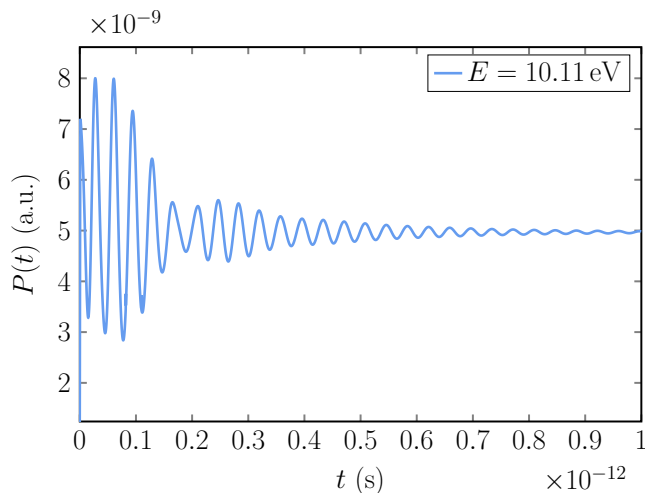


FIG. 8. Profile in time for two vibrational states within the resonance state and one vibrational state within the final state (similar to Figure 6) for  $q = 10$ , evaluated at a kinetic energy of 10.11 eV. A few data points which were affected by numerical noise have been discarded.

The resulting time-resolved spectrum is very similar to that for  $q = 1$  in Fig. 6. The Fourier analysis of the oscillation pattern evaluated at a kinetic energy of 10.11 eV and shown in Fig. 8 is, however, significantly different. It shows three different oscillations with periods 36.9 fs, 31.9 fs and 17.7 fs. The first two periods correspond to the two interferences of the two different vibrational resonance pathways with the direct pathway. The one with a period of 17.7 fs however corresponds to the resonance-resonance interference, which from the energy difference is expected to have a period of 17.2 fs.

### 3. Small energy splitting between the vibrational resonance states, $q = 10$

Until now, we have seen scenarios in which the vibrational resonance states were well separated in energy. However, this is not necessarily the case, and even most likely not. Using the parameters #5 given in Table I yields an energy difference for the vibrational resonance states of 0.0191 eV. As in section IV D 2 we have chosen a larger Fano parameter of  $q = 10$  in order to both narrow the individual peaks and increase the contribution of the resonance pathways. Nevertheless, the corresponding peaks in the spectrum cannot be resolved, as shown in Figure 9.

However, if the contributions of the resonance parts of the wavefunction are substantial, the resonance-

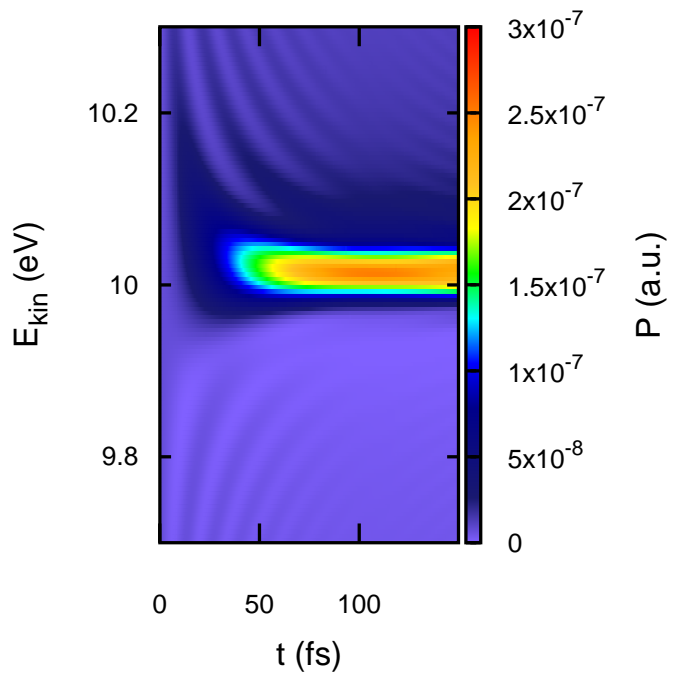


FIG. 9. (Colour online) Time-resolved RICD spectrum for two energetically close vibrational states in the electronic resonance state and a single vibrational state in the electronic final state for  $q = 10$ .

resonance interference can in principle be observed at energies that are different from the kinetic energy corresponding to the resonance and hence be distinguished from direct-resonance interferences. Furthermore, from the oscillation period of the signal, the energy difference between the two resonance states can be determined.

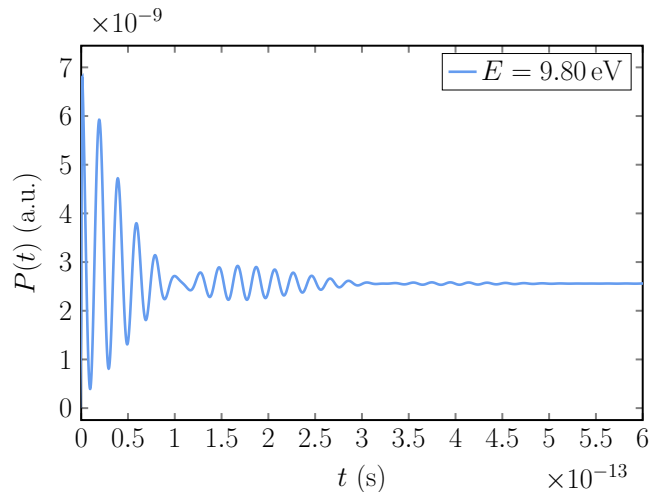


FIG. 10. Profile in time for two energetically close vibrational states within the resonance state and one vibrational state within the final state for  $q = 10$  (Figure 9), evaluated at a kinetic energy of 9.80 eV. A few data points which were affected by numerical noise have been discarded.



In Figure 10, we give an example for such an oscillatory variation in signal intensity for the parameter set #5 at a kinetic energy of 9.8 eV. It shows two oscillations. On the one hand, the oscillation with a period of 21 fs is caused by the interference of the direct term with either of the resonance ones. Since they are energetically so similar, the difference in the oscillation periods is not visible. It is only in the Fourier-transformed signal that a double peak can be seen, corresponding to oscillation periods of 18.7 fs and 20.9 fs, respectively. On the other hand, the oscillation with the longer period of ca. 220 fs is caused by the resonance-resonance interference.

We note that it may be experimentally difficult to resolve these variations in signal intensities in low intensity areas.

### E. Case 5: 2 vibrational bound states in the resonance state and 2 vibrational bound states in the final state

#### 1. Large energy splitting between the vibrational resonance states

In this case, the parameters #6 of Table I were used for the simulation. Both the resonance and the final state support two vibrational bound states. This is the smallest possible case in which all hitherto discussed properties are combined. The energy differences of the vibrational states are 0.2434 eV for the resonance state and 0.0493 eV for the final state.

These parameters lead to the spectrum shown in Figure 11. It is characterized by two large peaks, which are split into the two peaks for the different vibrational final states.

Since the energy difference between the two vibrational final states is very small, the width of the overall peak is hardly affected by their presence.

The Franck-Condon overlaps for the transition between the ground and the final state relevant for the direct pathway are  $\langle\chi_{\mu=0}|\chi_0\rangle = 0.60$  and  $\langle\chi_{\mu=1}|\chi_0\rangle = 0.49$ , which indicates that the direct pathways contribute with similar weights. The Franck-Condon overlaps relevant for the decay from the resonance states are more interesting. They are  $\langle\chi_{\lambda=0}|\chi_0\rangle = 0.40$ ,  $\langle\chi_{\lambda=1}|\chi_0\rangle = 0.33$ ,  $\langle\chi_{\mu=0}|\chi_{\lambda=0}\rangle = 0.87$ ,  $\langle\chi_{\mu=1}|\chi_{\lambda=0}\rangle = -0.27$ ,  $\langle\chi_{\mu=0}|\chi_{\lambda=1}\rangle = 0.37$ , and  $\langle\chi_{\mu=1}|\chi_{\lambda=1}\rangle = 0.57$ . Hence, the peak intensities and shapes are affected, in accordance with decreased effective Fano  $q$  parameters. Moreover,  $\langle\chi_{\mu=1}|\chi_{\lambda=0}\rangle$ , the Franck-Condon overlap between the vibrational ground state of the resonance state and the vibrational excited state of the final state, is negative and so is the corresponding effective Fano parameter. Under sign change of the effective  $q$  parameter, the peak shape becomes its own mirror image, which therefore explains the unexpected behaviour for the peak at 9.95 eV. In this particular example, its minimum coincides with the minimum of the neighbouring peak and the

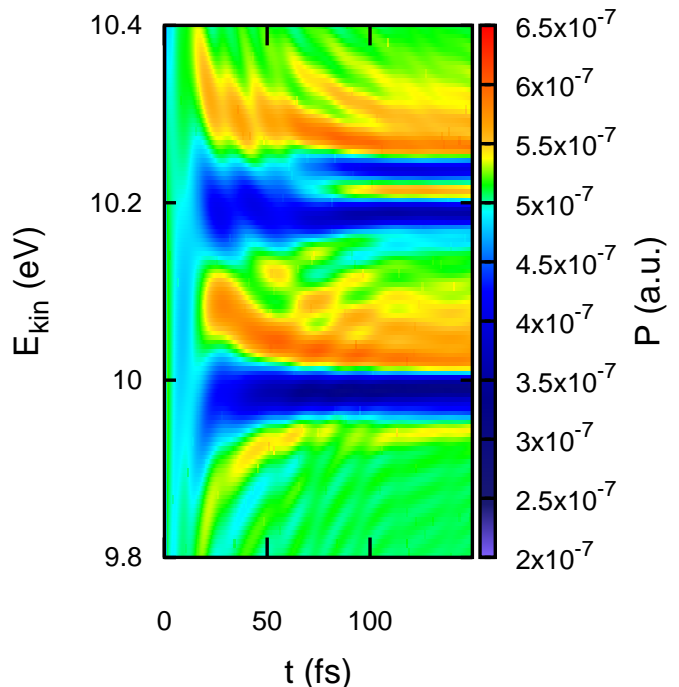


FIG. 11. (Colour online) Time-resolved RICD spectrum for two vibrational states in both the electronic resonance and final state with a large energy difference between the vibrational resonance states and a small energy difference between the vibrational final states.

typical Fano lineshape becomes more difficult to identify.

At a kinetic energy of 10.02 eV, an interference pattern is present that includes an oscillation with an apparent period of ca. 21 fs. Fourier analysis reveals this to be in fact two oscillations with periods of 19 fs and 24 fs, respectively, which are too close for the two oscillations to be distinguishable in the time-resolved signal. The energy difference between the vibrational resonance states relates to an oscillation with a 17 fs period, which fits nicely. However, the signals corresponding to direct-resonance interference that involves the vibrational excited state of the resonance state indicate oscillations with periods of 19 fs and 24 fs for  $\mu = 0, 1$ , respectively. An unambiguous attribution of the observed oscillations to the underlying pathways that give rise to them is therefore impeded: The interference pattern is obviously more complicated than in case 4 due to the manifold of different contributions for any chosen kinetic energy.

#### 2. Small energy splitting between the vibrational resonance states

When the parameters of the resonance- and the final-state potentials are interchanged (parameters #7 of Table I), the energy difference between the two resonance states becomes very small and the two larger signals are clearly separated from another as illustrated in Figure 12.

This may allow for an easier interpretation of the interference spectrum.

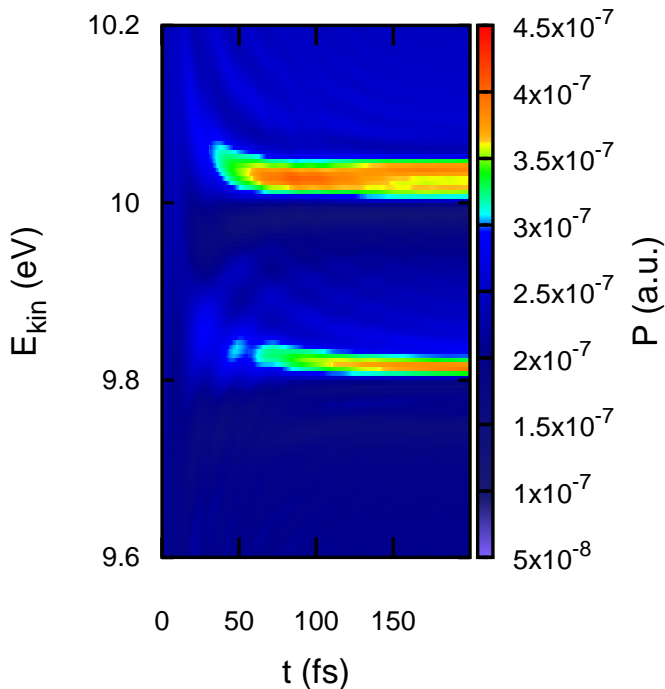


FIG. 12. (Colour online) Time-resolved RICD spectrum for two vibrational states in both the electronic resonance and final state with a small energy difference between the vibrational resonance states and a large energy difference between the vibrational final states.

Compared to the spectrum in Figure 11, the different direct pathways boost only those parts of the spectrum where the peaks are. Due to the Franck-Condon overlaps of this example, one part of the double peak around 9.8 eV is hardly visible, and we will therefore focus on the other double peak. As in the first example of this case, the negative sign of  $\langle \chi_{\mu=0} | \chi_{\lambda=1} \rangle$ , the Franck-Condon overlap between the vibrational excited state of the resonance state and the vibrational ground state of the final state, leads to an unusual line shape for the peak around 10.04 eV. However, there is also a clear contrast to the previous example, in that the small energy difference between the two vibrational states of the resonance state and their approximately even contributions to the spectrum in the double peak around 10 eV should, according to Eqs. (42) and (50), lead to a clear oscillation pattern in time caused by the resonance-resonance interference with comparatively long periods.

Due to this long oscillation period, the resonance-resonance interference should already close to the peak maxima be distinguishable from the interference with the direct pathway. This allows an evaluation with more significant peak intensity. We therefore focus on the time-resolved pattern for a kinetic energy of 10.01 eV close to the  $0 \leftarrow 0$  peak, which is shown in Figure 13 after the first 145 fs. Upon first inspection, the signal can be de-

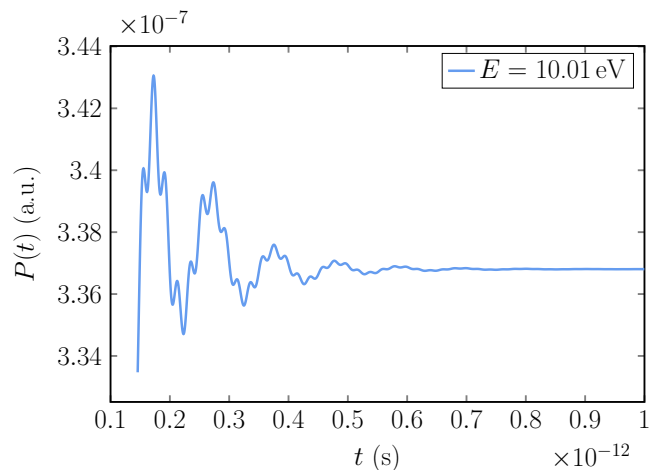


FIG. 13. Profile in time for two energetically close vibrational states within the resonance state and two energetically more distant vibrational states in the final state (Figure 12), evaluated at a kinetic energy of 10.01 eV. A few data points which were affected by numerical noise have been discarded.

scribed by two overlapping oscillations with very different frequencies, whose amplitude is decreased exponentially. A Fourier analysis of the signal shows that the dominant and the perturbing oscillation have periods of 100 fs and only 20 fs, respectively.

According to the absolute square of Eq. (42), five different kinds of oscillations could in principle be observable involving all possible combinations of vibrational states in the electronic resonance  $\lambda = 0, 1$  and final state  $\mu = 0, 1$  as well as the resonance-resonance contribution from the two different vibrational states  $\lambda = 0, 1$ .

The corresponding theoretical periods are given in Table II.

TABLE II. Oscillation periods for the different interference combinations.

#	characteristics	$T$ [fs]
1	$\mu = 0, \lambda = 0$	414
2	$\mu = 1, \lambda = 0$	16
3	$\mu = 0, \lambda = 1$	105
4	$\mu = 1, \lambda = 1$	20
5	$\lambda = 0, \lambda = 1$	84

The observed low-frequency oscillation is most likely inflicted by the interference between contributions from the vibrational excited resonance state and the vibrational ground state (parameters #3 of Table II), which also has a non-negligible contribution at 10.01 eV. The observed high-frequency oscillation can predominantly be attributed to the interference between the contributions from the two vibrational excited states (#4 of Table II), because the contributions from the pathway involving the vibrational ground state of the resonance state are disfavoured by the Franck-Condon overlaps. The oscillation

caused by the interference of the two resonance states decaying to the vibrational ground state is not visible, because the other contributions cover them.

## V. DISCUSSION

In this article, we have derived expressions for the time-resolved description of electronic decay processes including nuclear degrees of freedom. In the following, we would like to discuss the approximations and assumptions introduced in these derivations presented in section II.

1. We use the Born-Oppenheimer approximation throughout the article. Therefore, the derived expressions will not be applicable when strong non-adiabatic couplings exist which involve the resonance or the final states.
2. We assume that the transition dipole moment matrix elements  $\langle E|\mu|g\rangle$  are independent of the energy of the final state.
3. Such independence of the energy of the final state is also assumed for the coupling matrix elements  $V_{Er}$ . Consequently, the effective decay width  $W_\lambda$ , Eq. (12), is considered to be independent of energy.
4. In this article, we only consider bound vibrational eigenstates. Therefore, the introduced nuclear bases are not necessarily complete. This assumption manifests itself in the reduced overall decay widths (Eq. (12)) and therefore the observed increased lifetimes with respect to the purely electronic case. Moreover, these contributions are also missing in the simulated spectra. Their inclusion will be subject to future work.
5. In the above simulations, we discussed time-resolved spectra involving multiple resonance states in combination with several final states. In a rigorous treatment, it is only possible to include either several resonance or several final states, but not several states of both kinds. In order to still treat their combination, we have introduced a few approximations, whose impact we would like discuss in more detail.

- (a) In the derivation of the coefficients of the Fano wavefunction, we assume that different resonance states do not couple via the continuum. In this case, the only meaningful contribution in Eq. (10) is the one for  $\lambda' = \lambda$ . Phenomenologically, this means that no lifetime sharing between the different vibrational states of the resonance state is possible. For the molecular Auger-Meitner process with large decay widths, this is in many cases a crude approximation. However, for the RICD

process with longer lifetimes, this approximation becomes feasible, as can, e.g., be estimated from the ICD process of the neon dimer [56].

- (b) We neglect the impact of  $F_{\mu'}(E)$ . Neglecting  $F(E)$  in the purely electronic solution for one resonance and one final state results in neglecting a small shift in the resonance energy, while the overall shape of the corresponding peak remains the same. This effect is more pronounced when several resonance states are involved. By neglecting  $F_{\mu'}(E)$ , we neglect shifts of all resonance energies, which can change the energy differences between them. Additionally, we also neglect changes in the respective decay widths and hence lifetimes. Strong couplings via the continuum will therefore lead to qualitatively different spectra than those shown in this article. In extreme cases for two resonance states, one resonance state can combine the entire decay capability of the system into itself, while the other state is stabilized. It would be beneficial to go beyond the current limitations in future work.
- (c) The approximation of negligible couplings of different resonance states via the continuum leads to an underdetermined expression in Eq. (16). We therefore assume equal contributions of  $|a_\lambda(E)|^2 W_\lambda (\pi^2 + |z(E)|^2)$  for all vibrational resonance states. This approximation is very likely incorrect. If the contributions for different  $\lambda$  are not equal, it will change the relative size of the different contributions and introduce additional prefactors for each resonance or indirect contribution. The overall shape of the equations would not change though.
6. In the Fano wavefunction, the coefficients  $b$  of the continuum states are expressed as sums of contributions of the resonance states, Eq. (19). In a fashion related to the above assumption, we neglect the contributions of all vibrational states  $|\chi_{\lambda'}\rangle$  of the resonance state in this description except the one where  $\lambda' = \lambda$ . This greatly reduces the complexity of the expressions and facilitates the integration necessary when evaluating the Fano matrix elements, Appendix A. The solution of these integrals including the contributions of other states  $|\chi_{\lambda'}\rangle$  with  $\lambda' \neq \lambda$  will be discussed in a future study.

## VI. SUMMARY

In this section, we want to summarize the general results presented in section IV within the approximations discussed in section V.

As we have previously shown in Ref. [31], the signal shape for a single decay is given by the convolution of the corresponding Fano lineshape and the Fourier transform of the envelope of the exciting laser pulse. If the mean photon energy of the laser diverges from the resonance energy, the decay peak is damped, compared to the same peak on resonance (see Figure 4 of Ref. [31]).

The Fano parameter  $q$  (see Eq. (46)) determines the relative contributions of the different pathways to the final signal, and hence, the larger  $q$  (the larger the relative contribution of the resonance pathway), the more the maximum is moved towards the kinetic energy corresponding to the resonance and the minimum of the characteristic Fano lineshape is moved to  $-\infty$  (see Eqs. (48, 49)). Hence, the lineshape becomes a Lorentzian convoluted with a Gaussian, a so-called Voigt profile. Furthermore, the smaller the decay width (the longer the lifetime), the less pronounced the Fano lineshape is, according to Eq. (46).

Specific to several possible final states in general, and vibrational final states in particular, are several direct pathways and, correspondingly, several peaks at kinetic energies lower than the decay between the vibrational ground states. This can clearly be seen in Figure 5, where the spectrum after 200 fs is compared between cases 1, 2 and 3.

Analogously, we compare the spectra 200 fs after the centre of the pulse for several vibrational resonance states in Figure 14. In this case, the kinetic energy increases with the vibrational quantum number of the decaying state.

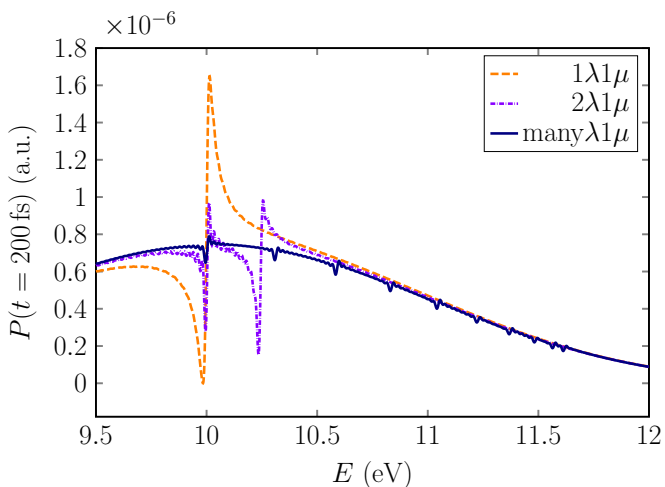


FIG. 14. (Colour online) Spectra at time  $t = 200$  fs for cases 1 (dashed curve in orange) and 4.1 (dash-dotted curve in violet) as well as a case with ten vibrational resonance states (solid curve in dark blue).

When several vibrational resonance states exist, all but one are automatically excited off-resonance, and hence, their resonance parts are weighted differently by the corresponding direct pathway, which can clearly be seen in

Figure 14.

The Fano lineshape is created by the interference between the contributions of the different pathways to the total wavefunction. As we have seen in all cases, this lineshape is affected by the inclusion of the nuclear degrees of freedom. The Franck-Condon overlaps alter the relative contributions of the different pathways and hence lead to different effective Fano parameters.

We have earlier shown in Ref. [31] that the interference between the different pathways is also responsible for the predicted oscillations in time and energy even for only one resonance and one final state. Inspection of Eq. (42) as well as Eqs. (43) and (44) infers that each vibrational resonance state contributes separately to the wavefunction. These contributions can therefore also interfere and cause additional time-dependent variations of the signals, which follow Eq. (50). The corresponding interference pattern can then be used to gather information about the wavepacket of the system and therefore the electronic and nuclear motion.

The resonance-resonance interference signal is only part of the overall signal. In order to observe it, one needs a system with a large  $q$  and to focus on energy regions with sufficient intensity but not at the kinetic energies corresponding to the resonance energies themselves. As discussed in case 4, a short initiating pulse can help creating the necessary peak intensity away from the kinetic energies of the electron corresponding to a resonant excitation.

The complexity of a spectrum as well as its time dependency is increased by the number of involved decaying and final states and so is the interference spectrum. In addition to the different interferences, overlapping signals can also lead to patterns which merely look similar to interference patterns. A Fourier analysis, though, can help to distinguish between overlapping signals and interference patterns, as we have discussed in detail in sections IV B and IV D.

## VII. ACKNOWLEDGEMENTS

E. F. and A. V. R. gratefully acknowledge funding through the Core Facility LISA<sup>+</sup> of the University of Tübingen. E. F. acknowledges the COST Action CA18222 (Attosecond Chemistry). We would further like to thank Nicolas Sisourat for a helpful comment on the completeness of our basis of vibrational states.

## Appendix A: Evaluation of the Fano matrix elements

The Fano integrals can now be solved by contour integration in the negative complex half-plane, where we employ Eq. (41), use  $\langle r|r \rangle = 1$ ,  $\langle E|E' \rangle = \delta(E - E')$  and  $\langle E|r \rangle = 0$  as well as  $\langle \chi_\lambda|\chi_{\lambda'} \rangle = \delta_{\lambda,\lambda'}$  and  $\langle \chi_\mu|\chi_{\mu'} \rangle = \delta_{\mu,\mu'}$  and furthermore ignore the effects of  $F_{\mu'}(E)$ :

$$\begin{aligned} & \langle \chi_\lambda | \langle r | U_F(t'', t') | r \rangle | \chi_{\lambda'} \rangle \\ &= \sum_{\lambda''} \int d\underline{E} \langle \chi_\lambda | \langle r | a_{\lambda''}(\underline{E}) | r \rangle | \chi_{\lambda''} \rangle \langle \chi_{\lambda'} | \langle r | a_{\lambda''}^*(\underline{E}) | r \rangle | \chi_{\lambda'} \rangle \exp[-i\underline{E}(t'' - t')] \end{aligned} \quad (\text{A1})$$

$$= \sum_{\lambda''} \int d\underline{E} \delta_{\lambda, \lambda''} \delta_{\lambda', \lambda''} a_{\lambda''}(\underline{E}) a_{\lambda''}^*(\underline{E}) \exp[-i\underline{E}(t'' - t')] \quad (\text{A2})$$

$$= \int d\underline{E} \exp[-i\underline{E}(t'' - t')] |a_\lambda(\underline{E})|^2 \delta_{\lambda, \lambda'} \quad (\text{A3})$$

$$= \int d\underline{E} \frac{\exp[-i\underline{E}(t'' - t')] W_\lambda}{N_\lambda ((\underline{E} - E_r - E_\lambda)^2 + \pi^2 W_\lambda^2)} \delta_{\lambda, \lambda'} \quad (\text{A4})$$

Note that the effective decay width  $W_\lambda$  is, according to Eq. (12), in principle dependent on the energy of the final state,  $W_\lambda = \sum_{\mu'} |V_{(\underline{E}-E_{\mu'})r}|^2 |\langle \chi_\lambda | \chi_{\mu'} \rangle|^2 = W_\lambda(\underline{E})$ . We now assume the electronic coupling matrix element  $V_{E_r}$  to be independent of the continuous kinetic energy of the emitted electron and to be sufficiently described by the discretized energy difference between the resonance and the final state and therefore denote it  $V_r$ . We incorporate the discretized final states by summing over them in the expression for the effective decay width, which now has become independent of the energy:  $W_\lambda(\underline{E}) = |V_r|^2 \sum_{\mu'} |\langle \chi_\lambda | \chi_{\mu'} \rangle|^2 = W_\lambda$ . Treating it as a constant inside the integral and evaluating the latter yields the Fano matrix element:

$$\frac{1}{N_\lambda} \delta_{\lambda, \lambda'} \exp[-i(E_r + E_\lambda - i\pi W_\lambda)(t'' - t')] \quad (\text{A5})$$

$$\begin{aligned} & \int dE'' \langle \chi_\lambda | \langle r | U_F(t'', t') | E'' \rangle | \chi_{\mu''} \rangle \\ &= \sum_{\lambda'', \bar{\mu}} \int dE'' \int d\underline{E} \int d\tilde{E} \exp[-i\underline{E}(t'' - t')] \langle \chi_\lambda | \langle r | a_{\lambda''}(\underline{E}) | r \rangle | \chi_{\lambda''} \rangle \langle \chi_{\bar{\mu}} | \langle \tilde{E} | b_{\tilde{E}, \bar{\mu}}^*(\underline{E}) | E'' \rangle | \chi_{\mu''} \rangle \end{aligned} \quad (\text{A6})$$

$$= \int dE'' \int d\underline{E} \exp[-i\underline{E}(t'' - t')] a_\lambda(\underline{E}) b_{E'', \mu''}^*(\underline{E}) \quad (\text{A7})$$

$$\begin{aligned} &= \int dE'' \int d\underline{E} \exp[-i\underline{E}(t'' - t')] a_\lambda(\underline{E}) \sum_{\lambda'} \left( \frac{V_{rE''} a_{\lambda'}^*(\underline{E}) \langle \chi_{\lambda'} | \chi_{\mu''} \rangle}{\underline{E} - E'' - E_{\mu''}} \right. \\ & \quad \left. + \frac{\underline{E} - E_r - E_{\lambda'}}{W_{\lambda'}} V_{rE''} a_{\lambda'}^*(\underline{E}) \delta(\underline{E} - E'' - E_{\mu''}) \langle \chi_{\lambda'} | \chi_{\mu''} \rangle \right) \end{aligned} \quad (\text{A8})$$

$$\begin{aligned} &= \int d\underline{E} \exp[-i\underline{E}(t'' - t')] a_\lambda(\underline{E}) \sum_{\lambda'} \left( a_{\lambda'}^*(\underline{E}) \langle \chi_{\lambda'} | \chi_{\mu''} \rangle \mathcal{P} \int dE'' \frac{V_{rE''}}{\underline{E} - E'' - E_{\mu''}} \right. \\ & \quad \left. + \frac{\underline{E} - E_r - E_{\lambda'}}{W_{\lambda'}} V_{r(\underline{E}-E_{\mu''})} a_{\lambda'}^*(\underline{E}) \langle \chi_{\lambda'} | \chi_{\mu''} \rangle \right) \end{aligned} \quad (\text{A9})$$

We again assume the coupling matrix element  $V_{E_r}$  to be independent of the final state,  $V_{E_r} = V_r$  and  $V_{rE} = V_r^*$ . Then the principal value of the integral in the first summand is zero. Furthermore, the effective decay width again becomes independent of the energy,  $W_\lambda(\underline{E}) = W_\lambda$ . The Fano matrix element then reads as

$$\int d\underline{E} \exp[-i\underline{E}(t'' - t')] V_r^* a_\lambda(\underline{E}) \sum_{\lambda'} \frac{\underline{E} - E_r - E_{\lambda'}}{W_{\lambda'}} a_{\lambda'}^*(\underline{E}) \langle \chi_{\lambda'} | \chi_{\mu''} \rangle. \quad (\text{A10})$$

Due to the sum over  $\lambda'$ , several terms contribute to the Fano matrix element. This renders further equations quite involved. Therefore, we make the assumption that the only vibrational eigenstate  $|\chi_{\lambda'}\rangle$  of the electronic resonance state  $|r\rangle$  that contributes to the description of the chosen final state  $|E''\rangle |\chi_{\mu''}\rangle$  is the chosen vibrational eigenstate  $|\chi_\lambda\rangle$ . This means that in Eq. (19) for the Fano coefficient of the final state,  $\delta_{\lambda, \lambda'}$  is introduced so that all  $\lambda'$  are replaced by  $\lambda$  and the sum over all  $\lambda'$  drops out. Since the present expression for the Fano matrix element has been derived by inserting Eq. (19) into Eq. (A7), the same is true here.

$$\int d\underline{E} \exp[-i\underline{E}(t'' - t')] V_r^* |a_\lambda(\underline{E})|^2 \frac{\underline{E} - E_r - E_\lambda}{W_\lambda} \langle \chi_\lambda | \chi_{\mu''} \rangle \quad (\text{A11})$$

$$= \frac{1}{N_\lambda} V_r^* \langle \chi_\lambda | \chi_{\mu''} \rangle \int d\underline{E} \frac{(\underline{E} - E_r - E_\lambda) \exp[-i\underline{E}(t'' - t')]}{(\underline{E} - E_r - E_\lambda)^2 + \pi^2 W_\lambda^2} \quad (\text{A12})$$

$$= -\frac{i\pi}{N_\lambda} V_r^* \langle \chi_\lambda | \chi_{\mu''} \rangle \exp[-i(E_r + E_\lambda - i\pi W_\lambda)(t'' - t')] \quad (\text{A13})$$

- 
- [1] I. Orfanos, I. Makos, I. Lontos, E. Skantzakis, B. Förg, D. Charalambidis, and P. Tzallas, *APL Photonics* **4**, 080901 (2019).
- [2] L. Meitner, *Z. Phys.* **9**, 131 (1922).
- [3] P. Auger, *C. R. Acad. Sci.* **177**, 169 (1923).
- [4] L. S. Cederbaum, J. Zobeley, and F. Tarantelli, *Phys. Rev. Lett.* **79**, 4778 (1997).
- [5] M. P. Seah, *Surf. Interface Anal.* **9**, 85 (1986).
- [6] M. Drescher, M. Hentschel, R. Kienberger, M. Uiberacker, V. Yakovlev, A. Scrinzi, T. Westerwalbesloh, U. Kleineberg, U. Heinzmann, and F. Krausz, *Nature* **419**, 803 (2002).
- [7] O. Smirnova, V. S. Yakovlev, and A. Scrinzi, *Phys. Rev. Lett.* **91**, 253001 (2003).
- [8] I. Babushkin, Á. J. Galán, J. C. de Andrade, A. Husakou, F. Morales, M. Kretschmar, T. Nagy, V. Vaičaitis, L. Shi, D. Zuber, L. Bergé, S. Skupin, I. A. Nikolaeva, N. A. Panov, D. E. Shipilo, O. G. Kosareva, A. N. Pfeiffer, A. Demircan, M. J. J. Vrakking, U. Morgner, and M. Ivanov, *Nature Physics* **18**, 417 (2022).
- [9] G. Greczynski and L. Hultman, *Prog. Mater. Sci.* **107**, 100591 (2020).
- [10] R. Santra, J. Zobeley, L. S. Cederbaum, and N. Moiseyev, *Phys. Rev. Lett.* **85**, 4490 (2000).
- [11] U. Hergenhahn, *J. Electron Spectrosc. Relat. Phenom.* **184**, 78 (2011).
- [12] T. Jahnke, *J. Phys. B* **48**, 082001 (2015).
- [13] E. Fasshauer, *New J. Phys.* **18**, 043028 (2016).
- [14] P. H. P. Harbach, M. Schneider, S. Faraji, and A. Dreuw, *J. Phys. Chem. Lett.* **4**, 943 (2013).
- [15] I. B. Müller and L. S. Cederbaum, *J. Chem. Phys.* **125**, 204305 (2006).
- [16] C. Richter, D. Hollas, C.-M. Saak, M. Förstel, T. Miteva, M. Mucke, O. Björneholm, N. Sisourat, P. Slavíček, and U. Hergenhahn, *Nature Comm.* **9**, 4988 (2018).
- [17] N. V. Kryzhevoi and L. S. Cederbaum, *Angew. Chem. Int. Ed.* **50**, 1306 (2011).
- [18] S. D. Stoychev, A. I. Kuleff, and L. S. Cederbaum, *J. Am. Chem. Soc.* **133**, 6817 (2011).
- [19] N. V. Kryzhevoi and L. S. Cederbaum, *J. Phys. Chem. B* **115**, 5441 (2011).
- [20] B. Oostenrijk, N. Walsh, J. Laksman, E. P. Mansson, C. Grunewald, S. L. Sorensen, and M. Gisselbrecht, *Phys. Chem. Chem. Phys.* **20**, 932 (2018).
- [21] A. Bande, K. Gokhberg, and L. S. Cederbaum, *J. Chem. Phys.* **135**, 144112 (2011).
- [22] A. Bande, *J. Chem. Phys.* **138**, 214104 (2013).
- [23] P. Dolbundalchok, D. Peláez, E. F. Aziz, and A. Bande, *J. Comp. Chem.* **37**, 2249 (2016).
- [24] E. Alizadeh, T. M. Orlando, and L. Sanche, *Annu. Rev. Phys. Chem.* **66**, 379 (2015).
- [25] B. Boudaïffa, P. Cloutier, D. Hunting, M. A. Huels, and L. Sanche, *Science* **287**, 1658 (2000).
- [26] F. Martin, P. D. Burrow, Z. Cai, P. Cloutier, D. Hunting, and L. Sanche, *Phys. Rev. Lett.* **93**, 068101 (2004).
- [27] E. Brun, P. Cloutier, C. Sicard-Roselli, M. Fromm, and L. Sanche, *J. Phys. Chem. B* **113**, 10008 (2009).
- [28] E. Surdutovich and A. V. Solov'yov, *Eur. Phys. J. D* **66**, 206 (2012).
- [29] M. Wickenhauser, J. Burgdörfer, F. Krausz, and M. Drescher, *Phys. Rev. Lett.* **94**, 023002 (2005).
- [30] M. Wickenhauser, J. Burgdörfer, F. Krausz, and M. Drescher, *J. Mod. Opt.* **53**, 247 (2006).
- [31] E. Fasshauer and L. B. Madsen, *Phys. Rev. A* **101**, 043414 (2020).
- [32] U. Fano, *Phys. Rev.* **124**, 1866 (1961).
- [33] C. Greene, U. Fano, and G. Strinati, *Phys. Rev. A* **19**, 1485 (1979).
- [34] C. H. Greene, A. R. P. Rau, and U. Fano, *Phys. Rev. A* **26**, 2441 (1982).
- [35] C. H. Greene, A. R. P. Rau, and U. Fano, *Phys. Rev. A* **30**, 3321(E) (1984).
- [36] C. H. Greene and C. Jungen, in *Advances in Atomic and Molecular Physics*, Vol. 21, edited by D. R. Bates and B. Bederson (Academic Press, 1985) pp. 51–121.
- [37] U. Fano and A. Rau, *Atomic Collisions and Spectra* (Academic Press, 1986).
- [38] A. Kirrander, H. H. Fielding, and C. Jungen, *J. Chem. Phys.* **127**, 164301 (2007).
- [39] A. V. Riegel and E. Fasshauer, *Figures*, DOI: 10.6084/m9.figshare.24449554.v2 (2024).
- [40] M. Born and K. Huang, *Dynamical Theory of Crystal Lattices* (Oxford University Press, London, 1954).
- [41] M. Born and R. Oppenheimer, *Ann. Phys.* **389**, 457 (1927).
- [42] C. J. Ballhausen and A. E. Hansen, *Ann. Rev. Phys. Chem.* **23**, 15 (1972).
- [43] F. Mies, *Phys. Rev.* **175**, 164 (1968).
- [44] V. Averbukh, I. B. Müller, and L. S. Cederbaum, *Phys. Rev. Lett.* **93**, 263002 (2004).
- [45] K. Gokhberg, S. Kopelke, N. V. Kryzhevoi, P. Kolorenč, and L. S. Cederbaum, *Phys. Rev. A* **81**, 013417 (2010).
- [46] E. Fasshauer, M. Pernpointner, and K. Gokhberg, *J. Chem. Phys.* **138**, 014305 (2013).
- [47] E. Fasshauer, M. Förstel, S. Pallmann, M. Pernpointner, and U. Hergenhahn, *New J. Phys.* **16**, 103026 (2014).

- [48] ELDEST version 2.0.3, Programme for the time-resolved investigation of electronic decay processes (2020), written by E. Fasshauer, DOI:10.5281/zenodo.3700062.
- [49] A. V. Riegel and E. Fasshauer, Input files, DOI: 10.6084/m9.figshare.24450322.v1 (2024).
- [50] P. M. Morse, *Phys. Rev.* **34**, 57 (1929).
- [51] K. Scholz, *Z. Physik* **78**, 751 (1932).
- [52] C. L. Pekeris, *Phys. Rev.* **45**, 98 (1934).
- [53] J. P. Dahl and M. Springborg, *J. Chem. Phys.* **88**, 4535 (1988).
- [54] A. Kaldun, A. Blättermann, V. Stooß, S. Donsa, H. Wei, R. Pazourek, S. Nagele, C. D. Ott, C. Lin, J. Burgdörfer, and T. Pfeifer, *Science* **354**, 738 (2016).
- [55] V. Gruson, L. Barreau, A. Jimenez-Galan, F. Risoud, J. Caillat, A. Maquet, B. Carre, F. Lepetit, J.-F. Hergott, T. Ruchon, L. Argenti, R. Taieb, F. Martin, and P. Salieres, *Science* **354**, 734 (2016).
- [56] S. Scheit, L. S. Cederbaum, and H.-D. Meyer, *J. Chem. Phys.* **118**, 2092 (2003).